Portable Small UAV

Written by:

- Almog Dov
- Assaf Aloush
- Bar Ovadia
- Dafna Lavi
- Orad Eldar

Supervisor: Dror Artzi

August 2013

Abstract

This project deals with small portable UAV, single-man operated and uses for over-the-hill observation.

The process began with market survey, comparison to other existing models and selection of a concept.

The chosen concept is a flying wing - for vertical takeoff and landing as for straight and level flight.
 The UAV is propelled using 3 motors, located in holes inside the fuselage, and a rear motor with pusher propeller
This is innovatory - using two independent propulsion systems: One for the vertical lift and one for the straight and level flight.

After development of the concept, choosing systems and components has been made. Aerodynamic analysis was based on theory and verified by a wind tunnel experiment.

Two tests have been conducted - A thrust test for the chosen motor and propeller and a wind tunnel test for the entire model.

One of the major problems dealt with was the cavity closing mechanism.
Since the concept includes holes in the wing, closing mechanism is needed.
Two options were considered, and a shutter mechanism has been chosen.

Final result is a flying wing, 4.5Kg weight and 1.8m wingspan, carried by 3 horizontal electric motors and one vertical electric motor, carrying a 99gr payload – NextVision MicroCam-D system.
The UAV has VTOL and fixed wing capabilities which allows flight time of 30 minutes.

This report includes all the information, considerations and thoughts during 2 semester period.

Index

1. Introduction

The aim of this project was designing an unmanned aerial vehicle under costumer's specifications. It included

An unmanned aerial vehicle (UAV) is an aircraft without a human pilot on board. Its flight is controlled either autonomously by computers in the vehicle, or under the remote control of a pilot on the ground.

Table 1 presents the categories of UAVs divided by mass, range, flight altitude and endurance.

Category name	Mass [kg]	Range [km]	Flight Altitude [m]	Endurance [hours]
Micro	< 5	< 10	250	1
Mini	<25/30/150	< 10	150/250/300	< 2
Close Range	25 −150	10 − 30	3000	2 − 4
Medium Range	50 −250	30 − 70	3000	3 − 6
High Alt. Long Endurance	> 250	> 70	> 3000	> 6

Table 1

There is a wide variety of shapes, sizes, configurations, and characteristics of UAVs. They are deployed predominantly for military and special operation applications, but also used in a small, yet growing number of civil applications. Such applications are policing, firefighting and nonmilitary security work such as surveillance of pipelines. UAVs are often preferred for missions that are too "dull, dirty or dangerous" for manned aircraft.

Figure 1

4

2. Customer Specification and Requirements

These are the costumer specification and requirements for the UAV:

- o Man-portable UAV

- o Over the hill / Urban surveillance

- o Fast field deployment

- o Endurance: 30 min

- o Simple, operated by one man

- o Real time video camera

- o Quiet

- o Portable Ground Control System (PGCS)

- o Fully automated flight (including take-off and landing)

3. Market survey

Since the costumer's requirements specified a small UAV that can be operated by one, unskilled man, the market survey has focused in two main categories: mini-UAVs and micro-UAVs.

Table 2 presents the survey of mini-UAVs. It can be seen that the majority of UAVs in the survey weight about 6-7 Kg and are launched with a catapult. Moreover, most UAVs have an electric propulsion system and can be recovered with parachutes or airbag. It also can be seen that all payload weight are about 1Kg.

Model	Skylark I-LE	Orbiter 1	Bird-Eye 400	Skylite B
Picture				
Manufacturer	Elbit	Aeronautics	IAI	Rafael
MTOW	7Kg	7Kg	4.1Kg	6Kg
Wingspan	3m	2.2m	2m	2.4m
Endurance	3hr	2hr	1.3hr	1.5hr
Payload	Day & night	Day & Night	Day & Night	Day & Night
Payload weight	1.2Kg	1.5Kg	1.2Kg	0.9Kg
Propulsion	Electric	Electric	Electric	Electric
Type of launch	Hand launch	Catapult	Catapult	Catapult
Recovery	Parachute	Parachute +Airbag	Parachute	Parachute +Airbag

Table 2

Table 3 presents the survey of micro-UAVs which also includes 'toys' like the Parrot. It can be seen that most of the UAVs weight about 0.5 Kg.

Model	Parrot	Mosquito	RQ11 Raven
Picture			
Manufacturer	A.R Drone	IAI	AeroVironment
MTOW	0.4Kg	0.5Kg	2.3Kg
Wingspan	N/A	35cm	1.4m
Endurance	Few minutes	40min	75min
Payload	HD video + WiFi	Miniature camera	Day & Night
Payload weight	N/A	N/A	200g

Table 3

As seen in table 3, the Parrot, which is a toy, has unique properties such as different number of motors. It is not a military of commercially grade product. Yet, it was decided to adapt some of its properties to be used in the UAV.

4. Conceptual approach selection

The conceptual approach was based on analysis of the customer specifications and requirements as well as the market survey.

The requirement for a single operator resulted in a small UAV with no launcher in order to make the UAV easy to carry. Moreover, the requirement for an unskilled operator led to an automated flight with safe take-off and landing to prevent faults during operating. Furthermore, the costumer's request for a simple recovery rejected the option of using a parachute or an airbag. The above requirement resulted in a fully automated UAV with the ability of vertical take-off and landing. Despite this conclusion, the use in tilted rotor was rejected due to the complicated control system required to support it. As a result, it was decided to separate the propulsion system of level flight from the propulsion system of the vertical take-off and landing.

Another costumer's requirement was a UAV with capability to reach an out of sight target. This led to a necessity in fixed wing abilities in order to sustain a long distance flight.

All the above have formed an innovative idea as a students' project for a design of a UAV.

5. Initial sizing and weight estimation

The sizing began with vertical take-off and landing capabilities, which meant three motors in a triangle formation as can be seen in figure 2.
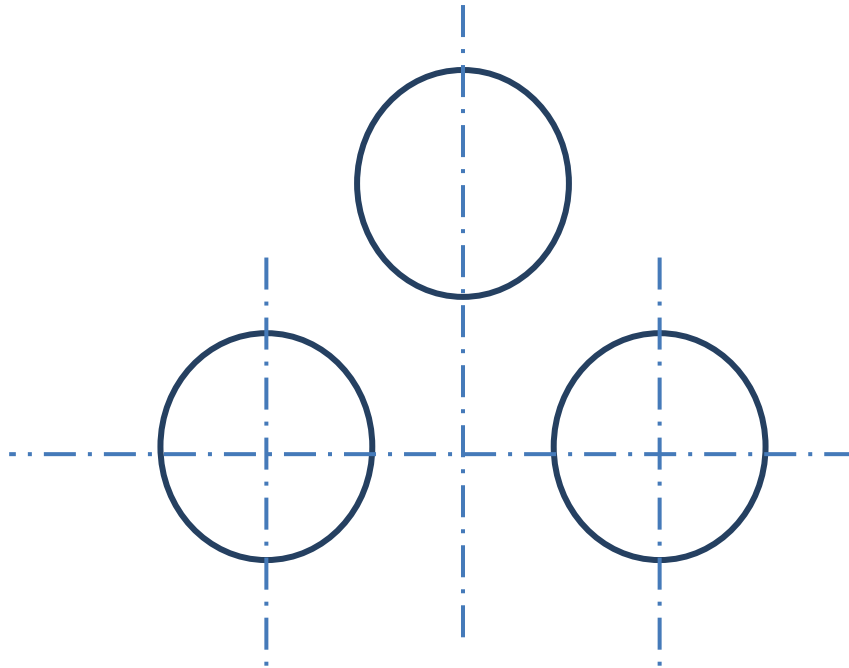
Figure 2

The configuration shown above could not fit into a fixed wing and therefore it was placed in a solid triangle (figure 3).
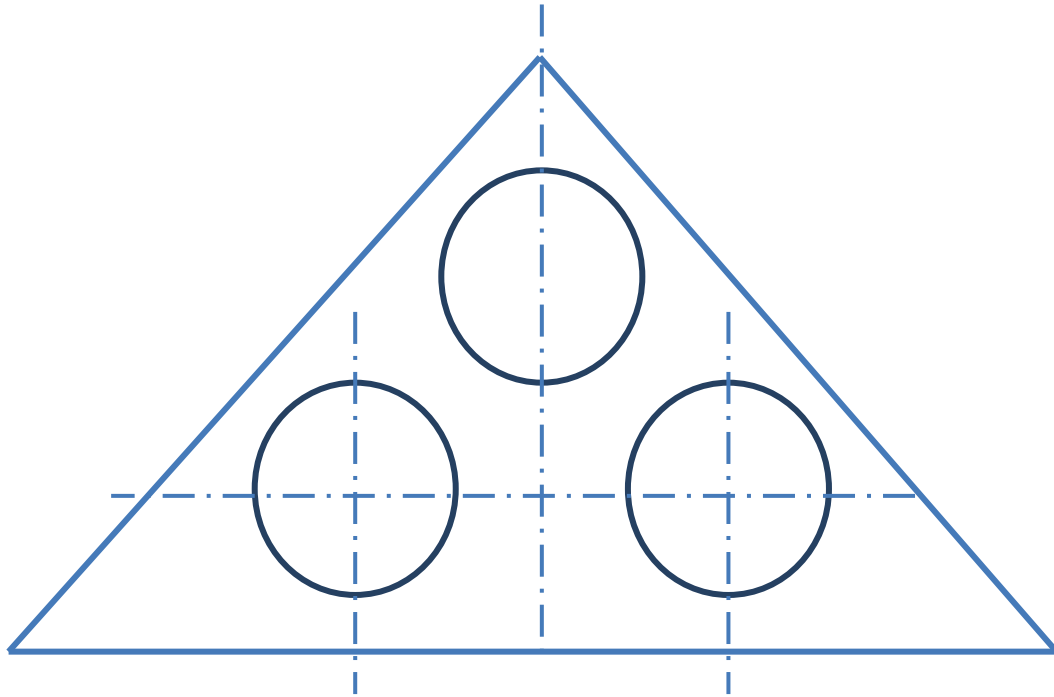
Figure 3

Two outer wings were added to the configuration in order to enlarge the aspect ratio and by that to optimize the performances of the UAV (figure 4).
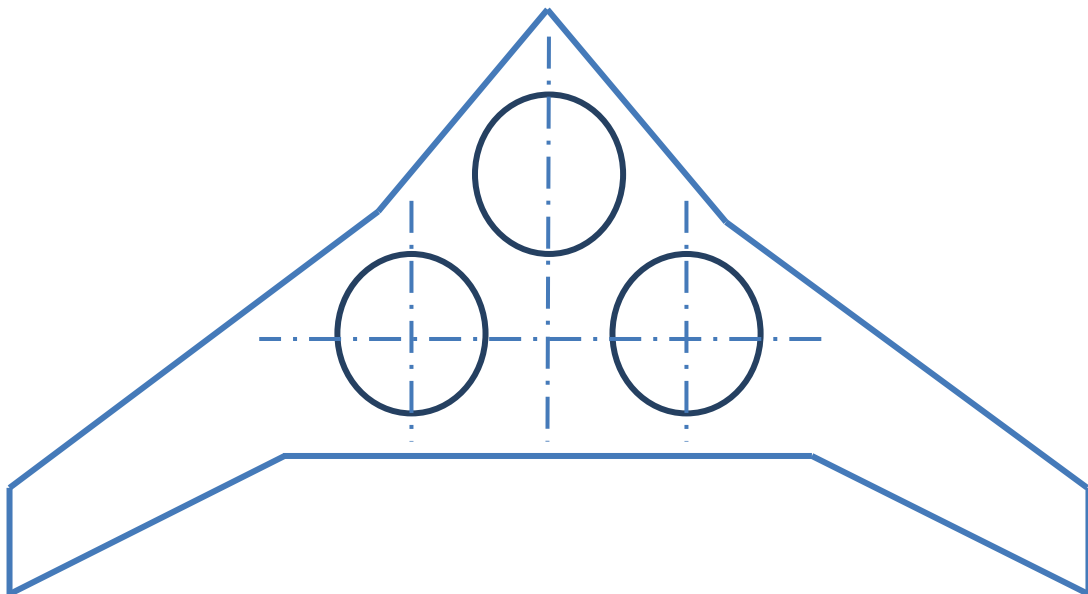
Figure 4

The configuration shown in figure 4 was chosen to be the final configuration and according to the market survey, we assumed a payload of 1Kg or less.

Next, using S.D Prior el al. article[1] (figure 5), the MTOW (Maximum take-off weight) for the required endurance (30 minutes) was estimated. A 1Kg payload was taken into consideration and due to the unique features of the UAV it was decided to add 0.5Kg to the resulting weight. Therefore, the resulting estimated payload weight was 4.5 Kg. It can be

seen in figure 5 that for $payload \cdot endurance = 1.5[Kg] \cdot 30[min] = 45[Kg \cdot min]$ the adequate MTOW is about 4Kg.

Figure 5

Table 4 presents the initial configuration and selection of main components, based on the market survey. It can be seen that the majority of weight is caused by the propulsion system. This is caused by the decision to use an electric propulsion system that required a powerful, and therefore heavy, motors and batteries.

Component	Estimated Weight
Structure	1.1Kg
Propulsion	3.0Kg
Avionics	0.3Kg
Payload	0.1Kg
Total	**4.5Kg**

Table 4

The total weight seen in table 4 was the first estimatiom of the MTOW is 4.5Kg.

6. Propulsion system selection

The selection of propulsion system was consisted of several choices regarding the system's properties. In order to choose the most suitable propulsion system, market surveys were conducted.

The first market survey focused on the differences between an electric motor and a two-stroke motor and indicated several advantages of the first motor over the later. First, the electric motor is considerably quieter than the two-stroke motor. Moreover, the electric motor has better weight-to-power ratio and battery-weight-to-endurance ratio. Furthermore, the electric motor requires low maintenance and has a low cost comparing to the two-stroke motor. As a consequence of the above indications, the electric motor was chosen for the propulsion system.

Next, a specific type of electric motor needed to be chosen and therefore a comparison was conducted between the brushed and brushless electric motors. The comparison showed multiple advantages of the brushless motor over the brushed. First of all, the brushless motor has high power to weight ratio and does not require a controller unlike the brushed motor. In addition, the efficiency of the brushless motor does not reduce due to friction caused by the brushes, while the efficiency of the brushed motor does. Moreover, in the brushed motor, the brushes have low lifetime since they are friction damages. In the brushless motor, however, there are no damages to the brushes. As a result of the advantages above, the brushless motor was chosen to be used in the UAV.

The brushless motor has two possible configurations: in-runner and out-runner. The comparison between the configurations is shown in table 5.

Property	In-runner	Out-runner
Efficiency	high	low
Noise level	loud	silent
Power	low	high

Table 5

It can be seen from table 5 that the out-runner has higher power and is quieter than the in-runner. The out-runner has lower efficiency, yet noise level and power are essential qualities to the UAV, therefore the out-runner was chosen.

7. Motor selection for vertical take-off and landing

The selection of propulsion system for vertical take-off and landing included a few decisions which followed a simple calculation based on a free body diagram (figure 6).
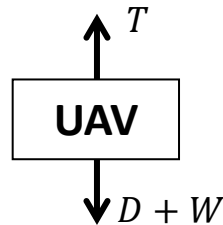

Figure 6

Where T represents the engine's thrust, D represents the drag on the UAV which is related to its surface and W represents the weight of the UAV.

To calculate the thrust each motor is required to supply, a safety factor was taken into account. Since a three motor configuration was chosen and the UAV's approximate weight is 4.5 Kg, the thrust each motor has to supply resulted in about 2.2 Kgf.

Under the decisions already made (brushless out-runner electric motor) a market survey of specific motors was conducted (table 6). The survey included the engines: Hacker a30-14L, OS OMA 3820-960, AXI 2820/8, AXI 2814/16 and Turnigy D3536/9 910KV. All motors were chosen under the limitation of 10 inch propeller which is the maximum diameter for the three holes.

Engine	Hacker a30-14L	OS OMA 3820-960	AXI 2820/8	AXI 2814/16	Turnigy D3536/9 910KV
Picture					
Thrust [Kgf]	2.41	2.13	2.13	2.56	1.87
Power [watt]	543	450	450	450	370
Weight [g]	143	160	151	151	102
Performance constant - Kv	800	960	860	860	910
Propeller diameter [inch]	10	10	10	10	10

Table 6

For the vertical take-off and landing, the Hacker a30-14L motor was chosen due to its high thrust and power, low K_V and weight.

8. Motor selection for level flight

In order to find the appropriate motor for level flight, the required power to overcome the drag was calculated. The Power and Drag equations that were used are the following:

$$P_{req} = \frac{1}{2}\rho S C_{D0} V^3 + \frac{2KW^2}{\rho S V}$$

$$D = \frac{1}{2}\rho S C_{D0} V^2 + \frac{2KW^2}{\rho S V^2}$$

Where P_{req} represents the required power, D represents the drag on the UAV, ρ represents the air density, S represents the reference surface, V represents the UAV's velocity, W represents the UAV's weight, C_{d_0} represents the drag coefficient and K is a combination of geometry parameters of the UAV. Furthermore, the values of S, C_{d_0}, K and W were taken from the UAV's geometry.

For a 4.5 kg aircraft and cruise speed of 30 m/s (approx. 58 knots), the calculated required power was 1214 Watt. According to the drag equation, the drag at that speed is approximately 2.5 Newtons.

A market survey was conducted to choose the most suitable motor. Since electrical motors generally use about 60% of their maximum power, the motors that were examined have maximum power of about 1600 Watt. Moreover, the survey focused on motors designed by Hacker and AXI, due to their good reputation in the UAV community.

For level flight, a crucial part of motor selection is the propeller. By using the right diameter and pitch of propeller, it is possible to fully utilize the motor according to the restrictions.

Using the following equations of power and thrust for propeller blades, the power required for the configuration and the thrust it yields were deduced.

$$P = D^5 \cdot RPM^3 \cdot \rho \cdot C_p \cdot N$$

$$T = D^4 \cdot RPM^2 \cdot \rho \cdot C_T \cdot N$$

Where D represents the propeller's diameter, RPM represents the rotational speed, C_p represents the propeller's power coefficient, C_T represents the propeller's thrust coefficient and N represents the number of blades coefficient. For 2 blades $N = 1$, for 3 blades $N = 1.4$ and for 4 blades $N = 1.7$.

In order to discern the flight time, the equation $P = VI$ was used. In can be seen that the more current a battery can hold the longer the UAV can stay in the air.

The motors that were included in the survey are presented in table 7.

Motor	Hacker A50 12-L	Hacker A50 14-L	AXI 4130-16
Picture			
Battery	6s	6s	6s
RPM	6440	5775	7161
Propeller	17x10	17x8	16x10
Power	1012 W	720 W	1106W
endurance	15 min	21 min	21min
Current needed	15 A	12A	18A
Total weight of motor + battery	3.3kg	2.8kg	3.8kg

Table 7

As seen in table 7, the recommended setup according to the motor manufactures yield good results. Yet, the weight of the batteries needed to sustain a 20 minutes flight is very high. This is due to the high power required. The solution was lowering the diameter of the propeller and by that lowering the power needed. The problem with the solution proposed is the cost of flight speed.

However, using 3 blades propeller with shorter diameter enables to reduce the power required to sustain fight while providing enough flight speed and thrust.

According to the motor analysis, the best motor for the aircraft is Hacker A50 14-L.

9. Propeller selection

9.1 Propeller selection for vertical take-off and landing

In order to minimize the effect on the UAV's performance, the motors' holes should be as small as possible. Therefore, the minimal propeller diameter needed to provide enough power for vertical take-off and landing was found using the thrust equations above.

3 motors were used to provide total thrust of 4.5Kgf. Each is required to provide thrust of 1.5Kgf. Figure 7 shows raw calculations of thrust vs. RPM for different propeller diameters and pitch angles.
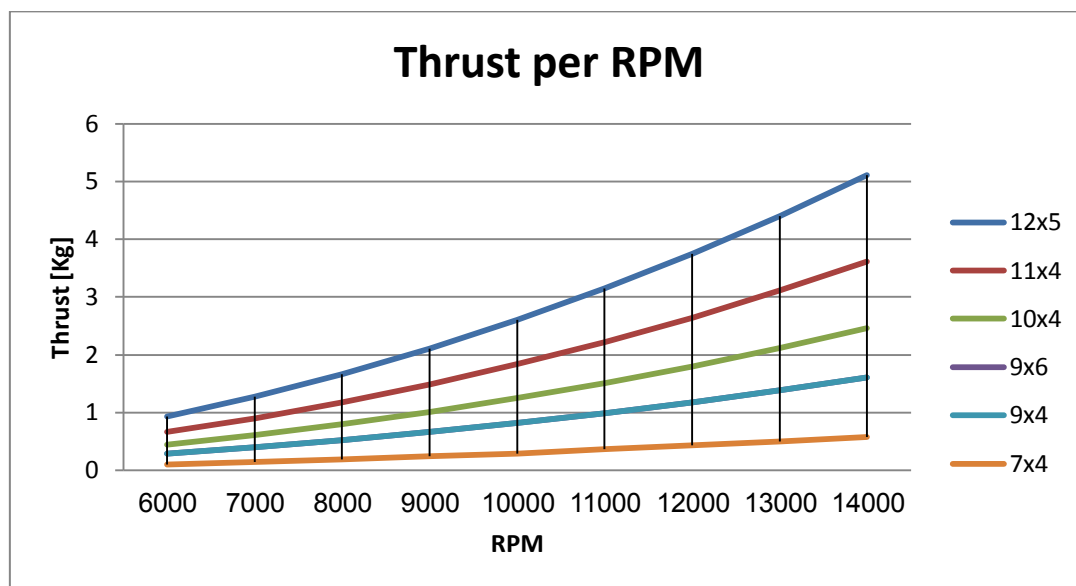
Figure 7

The reasonable RPM was deduced using the suggested motors for thrust of 1.5kgf. The RPM that was found was 10,000-11,000 and the optimal minimal diameter was 10 inches and 4 degrees pitch. Using a diameter of 9 inches may reduce the motor's holes in the body; however it may require much stronger motors which will require more power and, as a result, heavier batteries.

In the propeller thrust test the analysis was verified as a 10x4 propeller yielded slightly more thrust than 1.5kgf.

9.2 Propeller selection for level flight

Table 7 presents comparison between different propellers. This comparison was received after calculating the thrust, weight, required power and current for flight time of about 20 minutes. The calculation was based on the selected motor for level flight which had rotational speed of about 6200 RPM.

Prop size	2 blades				3 blades			
	Thrust [kg]	Req. power [W]	Total weight [kg]	Current needed [A]	Thrust [kg]	Req. power [W]	Total weight [kg]	Current needed [A]
15x8	2.64	520	2	8	3.7	728	2.1	9
15x10	2.64	650	2.1	9	3.7	911	2.7	12

Table 8

It can be seen in table 8 that a 3-blade propeller provides more current that the 2-blade propeller. Therefore, we optimized the propeller size and type to a 3-blade propeller with 15 inches diameter and 8 degrees pitch.

This configuration with the selected motor yields enough thrust to sustain flight speed of approximately 40 knots. This allows maintaining 20 minutes of flight with minimal power and minimal batteries weight.

10. Battery selection

Since an electric propulsion system was chosen, batteries are required for the motors.

First, several types of batteries were compared (table 9).

	NiCd – Nickel Cadmium	NiMH – Nickel Metal Hydride	Li-Ion – Lithium Ion	LiPo – Lithium Ion Polimer
Picture				
Nominal cell voltage [volt]	1.2	1.2	3.6	3.7
Specific power [Watt/Kg]	150	250-1000	250-340	Up to 7500

Table 9

As shown in table 9, the LiPo batteries have the highest nominal cell voltage and highest specific power. Therefore, LiPo batteries were chosen.

The selection of the batteries was based on the equation:

$$Pt = IV$$

Where P represents the power of the engine, t represents the endurance requirement of the UAV, and I and V represent the current and voltage of the battery, accordingly.

To calculate the current each battery is required to supply, the following values were used:

10.1 Batteries selection for vertical take-off and landing

For vertical take-off and landing three LiPo batteries are needed, one for each of the three Hacker motors that were chosen.

The power of each Hacker a30-14L motor: $P = 543 \ [Watt]$

The endurance requirement from the UAV: $t = \frac{4}{60} \ [Hour]$

The voltage supplied by a 4-cell LiPo battery: $V = 14.8 \ [Volt]$

The current required from each battery: $I = \frac{Pt}{V} \cong 2.45 \ [A \cdot Hour]$

Next, a market survey was conducted to compare several LiPo batteries which are able to supply current of $2.45 \ [A \cdot Hour]$ (table 10).

Battery Model	ZIPPY Compact I 300mAh 4S 35C	ZIPPY-K Flightmax 2500mAh 4S I P 20C	Thunder Power RC G6 Pro Lite 25C 2700mAh 4S	Genesis Power 4S 14.8V 2500mAh 40C
Capacity [Ah]	1.3	2.5	2.7	2.5
Weight [gr]	2x150	246	238	280
Dimensions LxWxH [mm]	78x34x29	116x33x37	102x34x34	136x44x23

Table 10

As shown in table 10, the Thunder Power battery has the highest capacity and has the lighter weight. Therefore, the Thunder Power RC G6 Pro Lite 25C 2700mAh 4S battery was chosen for vertical take-off and landing.

10.2 Battery selection for level flight

The power of Hacker a50-14L: $P = 700 \ [Watt]$

The endurance requirement from the UAV: $t = \frac{20}{60} \ [Hour]$

The voltage supplied by a 6-cell LiPo battery: $V = 22.2 \ [Volt]$

The current required from the battery: $I = \frac{Pt}{V} \cong 9 \ [A \cdot Hour]$

To supply the required current, it was decided to use two LiPo batteries, each required to supply current of $4500 \ [mA \cdot Hour]$.

A market survey was conducted to compare several LiPo batteries which are able to supply current of $4500 \ [mA \cdot Hour]$ (table 11).

Battery	Weight
Turnigy nano-tech 4500mah 6S 35~70C	676g
ZIPPY Compact 4500mAh 6S 35C	696g
Turnigy 4500mAh 6S 30C Lipo Pack	745

Table 11

The most important property is the weight of the battery, therefore the Turnigy nano-tech 4500mah 6S 35~70C battery was chosen for level flight.

11. Airfoil selection

The configuration of flying wing has several benefits for the UAV and therefore it was chosen. First, it provides enough space for the vertical propellers, which means the UAV can take-off and land vertically. Secondly, this configuration does not require a tail so the tail can be dismissed. Since a configuration with no tail is lighter than a one with a tail, the flying wing would have less weight than a standard UAV configuration. However, the absence of the tail causes two main problems – the wing has to achieve its own stability and there is also no place for the elevators and rudders.

In order to overcome the above problems it was decided to place the elevators on the wing itself, as shown in figure 8. Also, it was decided to add winglets to the configuration and place the rudders on them.
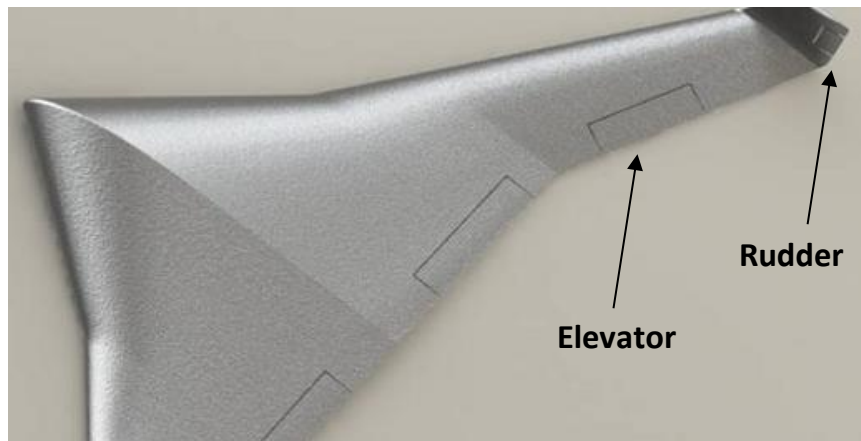
Figure 8

Next, it was necessary to stable the UAV. Stability was achieved by using a reflex profile (figure 9).
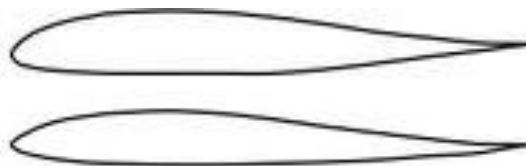
Figure 9

As shown in figure 9, the curve of the reflex profile twists upwards at the trailing edge. When the UAV has a positive AOA, the twist of the reflex profile causes a negative moment which counteracts to the AOA and stabilizes the UAV.

Several profiles were compared while the most critical property was the profile's thickness and lift-to-drag ratio (L/D).
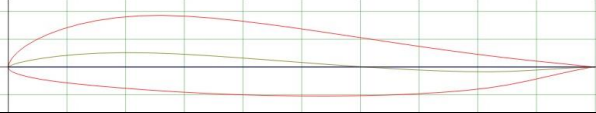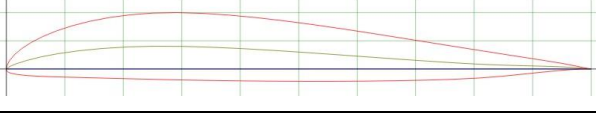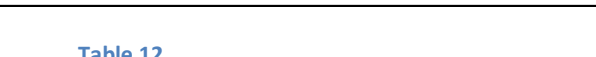
profile	Max t/c	picture
EPPLER E340	13.70%	
EPPLER E334	11.90%	
S5010	9.80%	
NACA M6	12%	
HS520	8.84%	
HS522	8.67%	

Table 12

As shown in table 12, the profiles EPPLER E340, EPPLER E334 and NACA M6 are the thickest.

Figure 10 shows the lift-to-drag ratio of the profile S5010. It can be seen that for Reynolds number of 200,000 the maximal ratio is 43.79. Also, for Reynolds number of 300,000 the maximal ratio is 52.73.
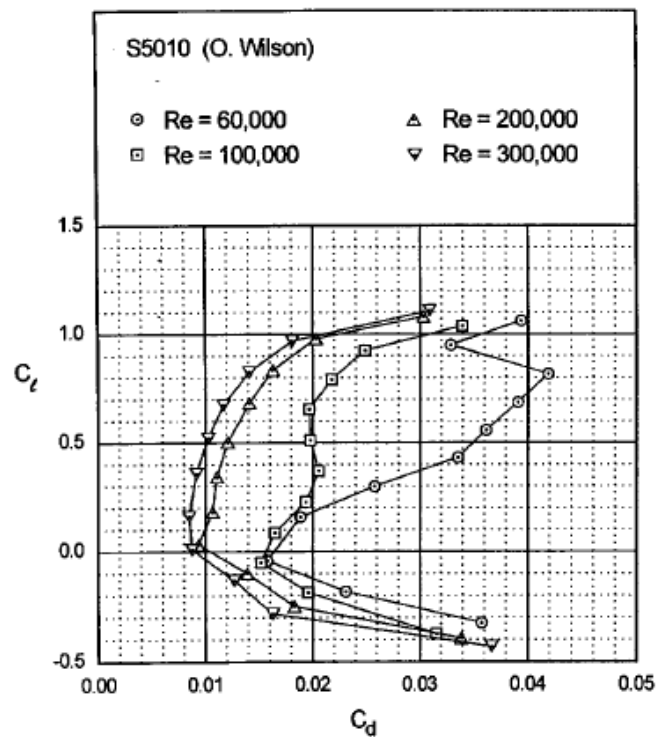

Figure 10

Figure 11 shows the lift-to-drag ratio of the profile HS522. It can be seen that for Reynolds number of 200,000 the maximal ratio is 62.89. Also, for Reynolds number of 400,000 the maximal ratio is 80.65.
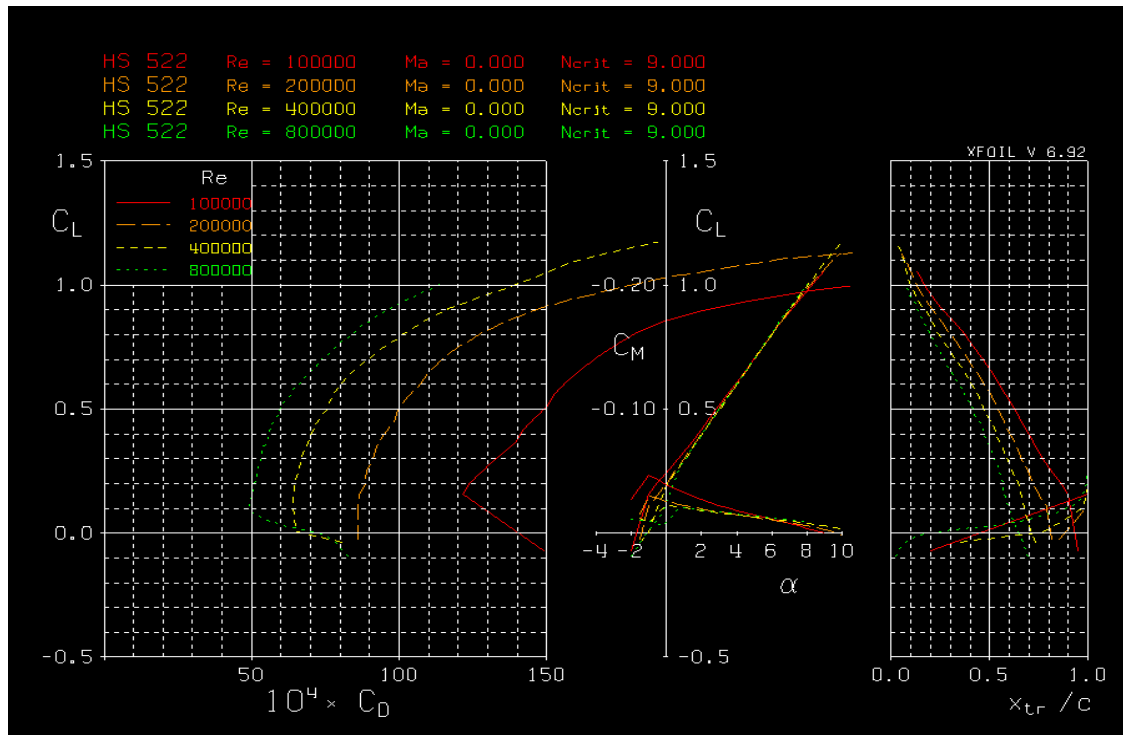

Figure 11

Figure 12 shows the lift-to-drag ratio of the profile HS520. It can be seen that for Reynolds number of 200,000 the maximal ratio is 53.85. Also, for Reynolds number of 400,000 the maximal ratio is 68.52.
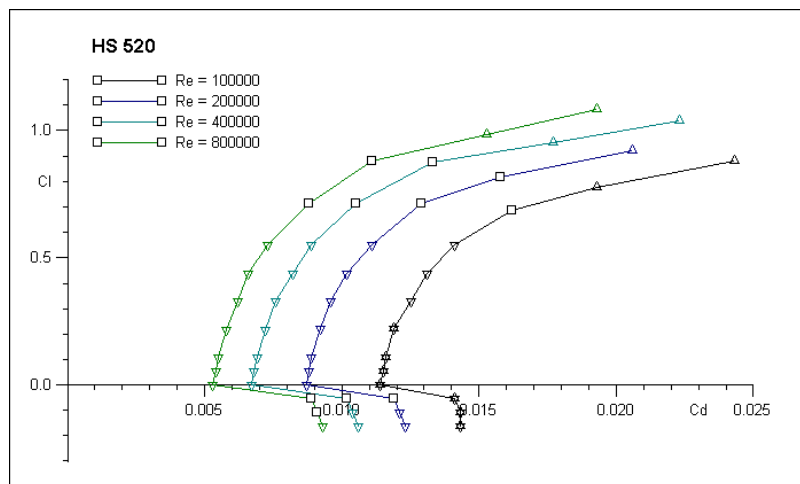

Figure 12

Figure 13 shows the lift-to-drag ratio of the profile EPPLER E340 which was taken from aerodesign.de. It can be seen that for Reynolds number of 200,000 the maximal ratio is 58.74. Also, for Reynolds number of 500,000 the maximal ratio is 80.32.
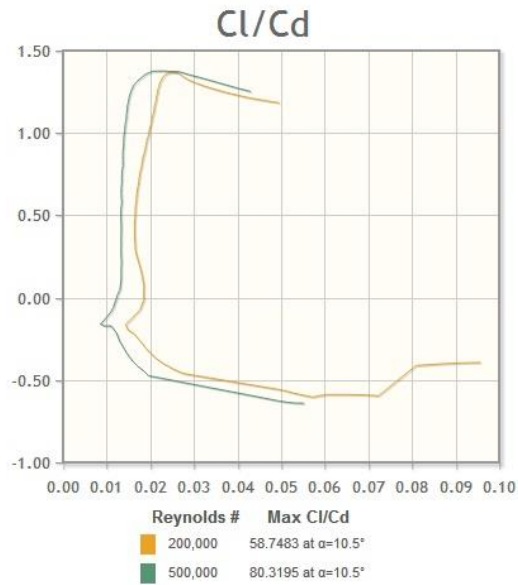
22

Figure 13

Figure 14 shows the lift-to-drag ratio of the profile EPPLER E334 which was taken from aerodesign.de. It can be seen that for Reynolds number of 200,000 the maximal ratio is 65.97. Also, for Reynolds number of 500,000 the maximal ratio is 100.83.
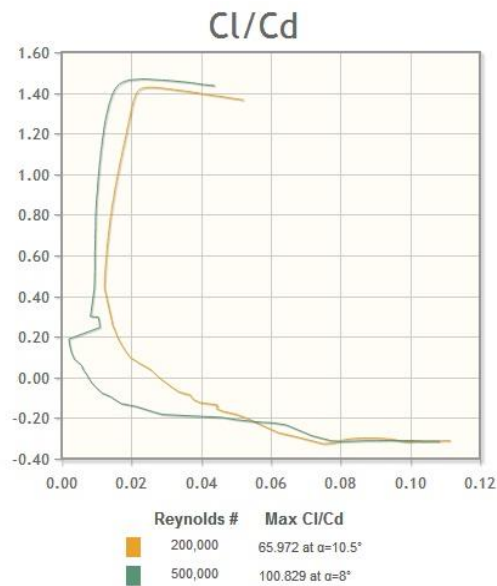

Figure 14

Figure 15 shows the lift-to-drag ratio of the profile NACA M6 which was taken from aerodesign.de. It can be seen that for Reynolds number of 200,000 the maximal ratio is 66.49. Also, for Reynolds number of 500,000 the maximal ratio is 87.40.
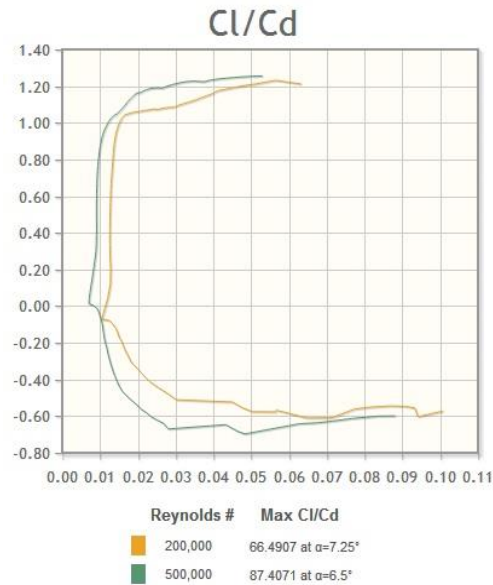
Figure 15

Next, all six profiles were analyzed with Xfoil program for Reynolds number of 300,000 which is the Reynolds number the UAV is planned to fly in. The following graphs were received:

Figure 16 shows the drag coefficient Vs. the AOA. It can be seen that EPPLER E340 and EPPLER E334 have the lowest drag coefficient for high and that for low AOA the drag coefficients of all profiles are approximately similar.
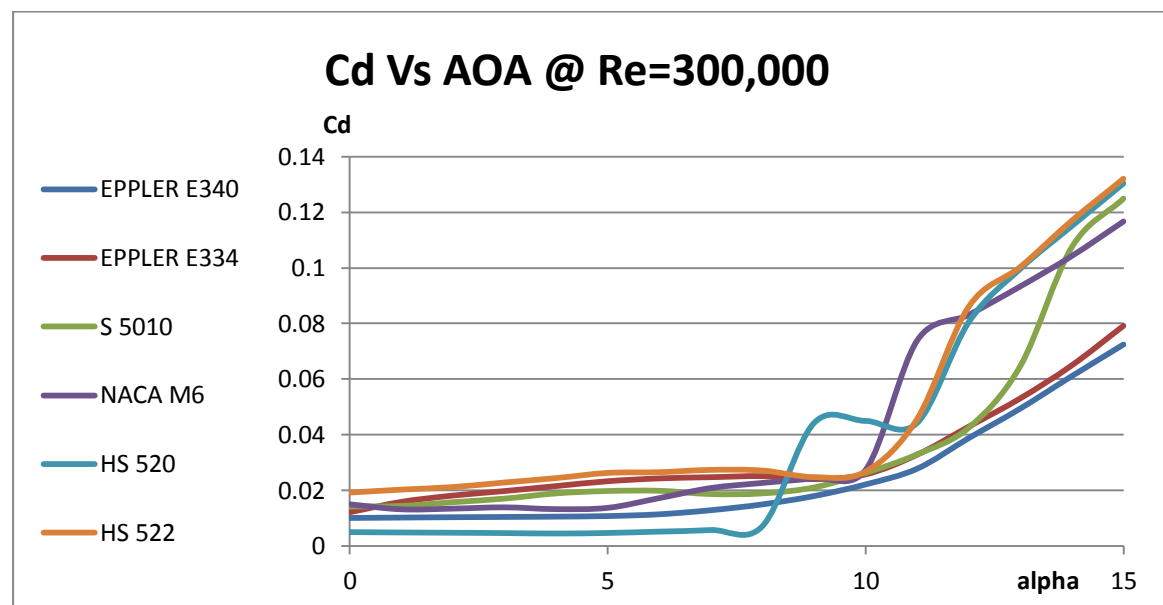

Figure 16

Figure 17 shows the moment coefficient Vs. the AOA. In order to reach stable UAV, C_m must be negative. It can be seen that EPPLER E334 has large negative moment coefficient. Moreover, all other profiles have negligible C_m.
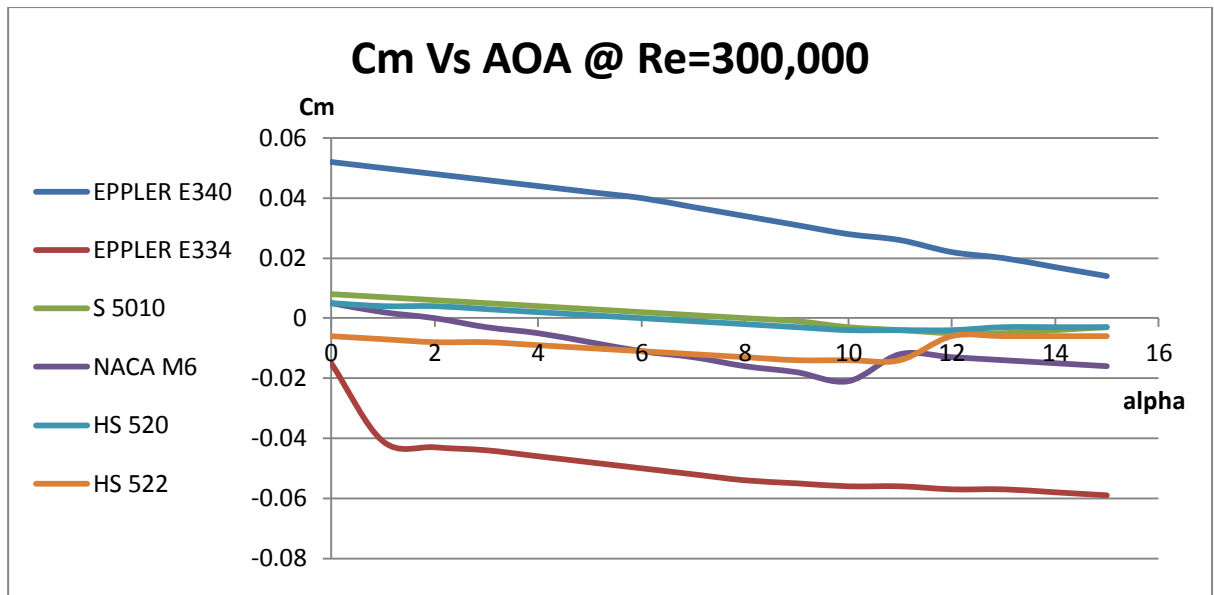
Cm Vs AOA @ Re=300,000

Figure 17

Figure 18 shows the lift coefficient Vs. the AOA. It can be seen that EPPLER E334 has highest lift coefficient and relatively high stall angle.
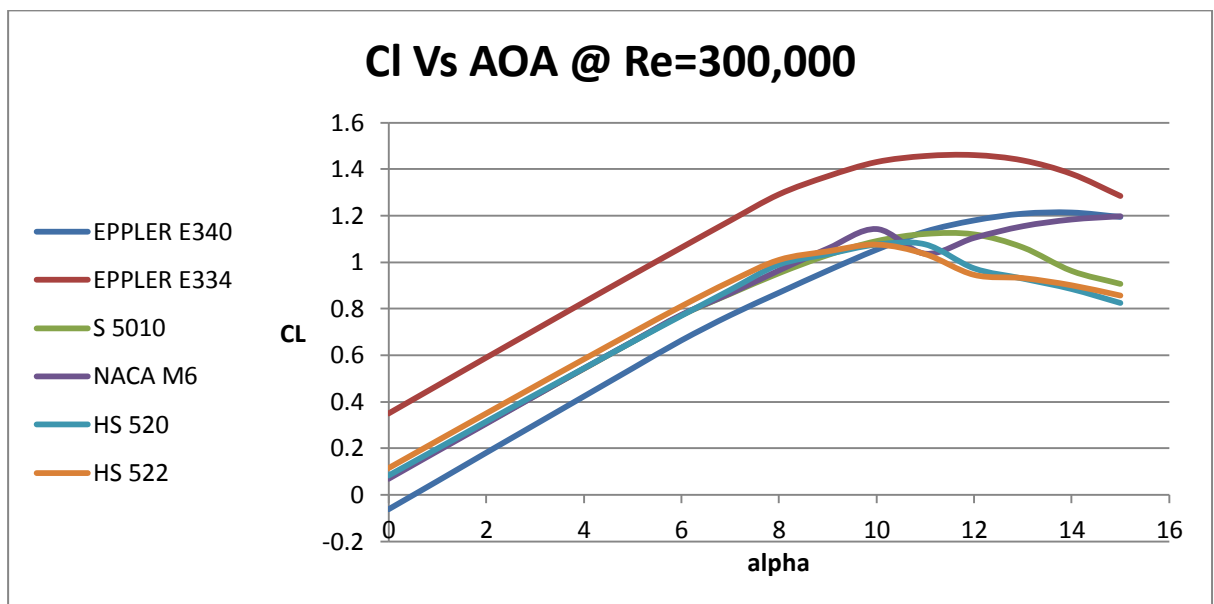

Cl Vs AOA @ Re=300,000

Figure 18

After summarizing all the results above, it was decided to use the EPPLER E334 profile especially due to its large thickness and high lift-to-drag ratio. Furthermore, the EPPLER E334 has low drag coefficient, the highest lift coefficient, a relatively high stall angle and a negative moment coefficient.

12. E/O Sensor selection

A market survey was conducted in order to choose the lightest sensor (table 13).

Model	D-STAMP	MicroPop	MicroCam D	VD/GD170
Picture				
Manufacturer	Controp	IAI	Nextvision	USA Vision
E.O Sensor	Day & Night	Day & Night	Day	Day & Night
Weight	1 Kg	700gr	99gr	900gr

Table 13

All sensors that were surveyed were too heavy and a compromise had to be made. Therefore, the chosen E/O sensor was the Nextvision MicroCam D. This sensor has light weight and satisfying performance, though it is only a day sensor rather than day&night.

13. Thrust test

In order to verify motor and propeller selection, a thrust test has been done.

Figure 19 shows the test setup: the motor and propeller connected to a weight that represents the UAV approximate weight. On the left, the chosen LiPo battery can be seen and on the right, the voltmeter is positioned. At the bottom of the picture, the RPM measurement device can be seen.

Figure 19

As shown in figure 19, the test included several propellers, some of 2-blades and some of 3-blades.

Figure 20

Table 14 presents the thrust test results. It can be seen that the selection of motor and propeller is satisfying. Though comparing to the prediction less thrust was received, the results were within the required limits of more than 1.5Kg.

Propeller [Diameter X Pitch]	Throttle [%]	Thrust [Kg]
APC 9X3.8	50	
	75	0.9
	100	1.05
APC 9X7.5	50	0.5
	75	1.05
	100	1.09
APC 10X4.7	50	0.77
	75	1.55
	100	1.59

Table 14

The errors during the test mainly resulted from the structure of the test mount. The torque produced by the motor was too strong for the mount structure which had a yaw tendency. In order to correct it, it was necessary to hand held the structure which distributed to the accuracy of the digital weight.

14. Preliminary performance analysis

In order to examine the aircraft performances, several analyses were carried out.

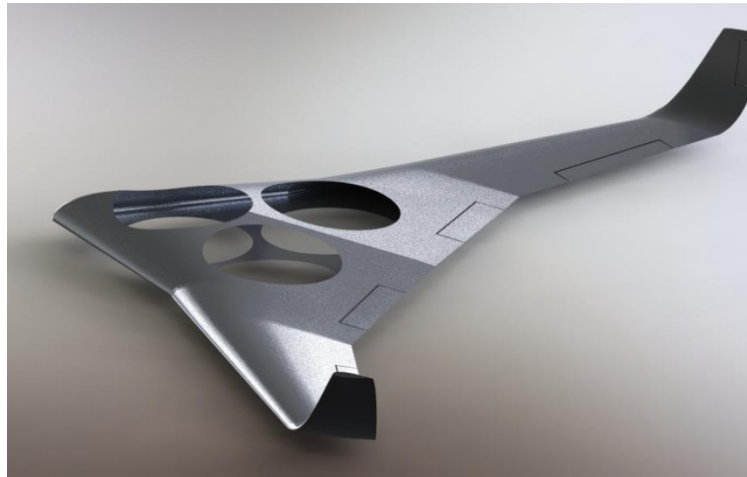First, a 3D model was designed using the selected airfoil and the program SolidWorks (figure 21).

Figure 21

14.1 CFD results:

A CFD analysis was carried out on the UAV, using the CFD option of the SolidWorks program (figure 22).
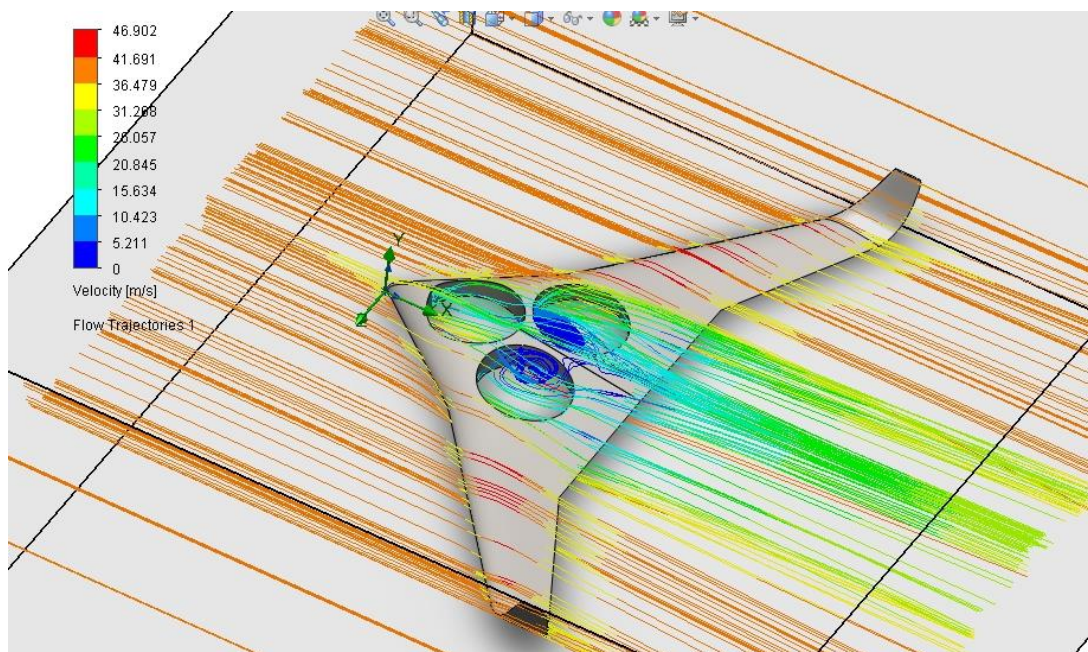

Figure 22

The results showed reasonable flow on the model, and turbulence flow on the cavities (figure 23). In order to examine the results, a closer look of the cavities is presented (figure 24).
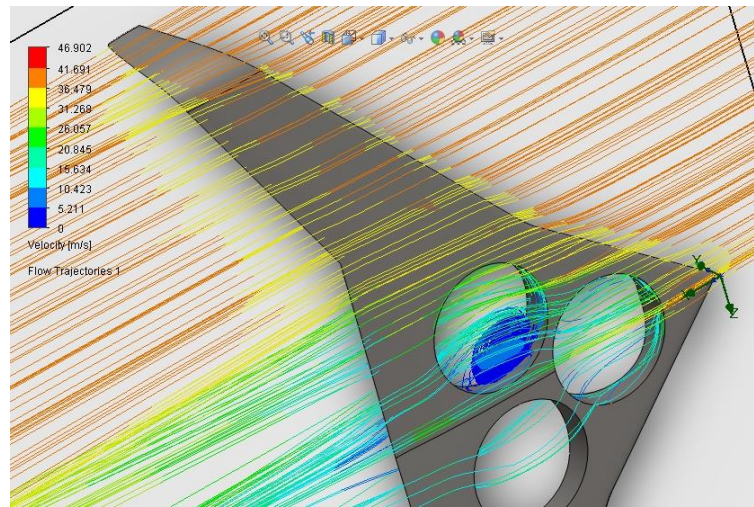

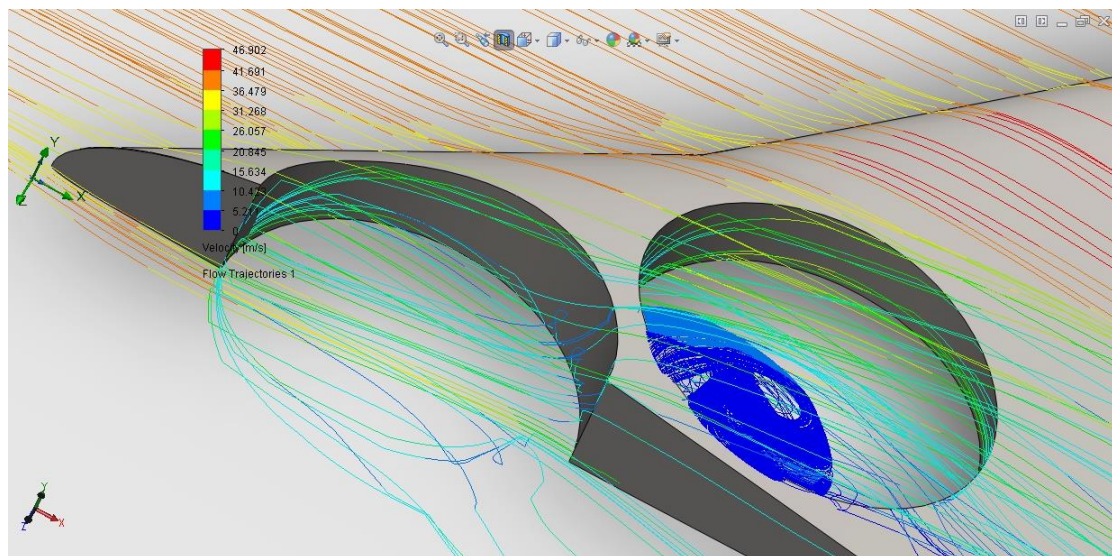Figure 23

Figure 24

After examining the CFD analysis results, it was concluded that the cavities of the aircraft led to turbulence and therefore, great loses in performances. The option of closing the cavities was then investigated (figure 25).
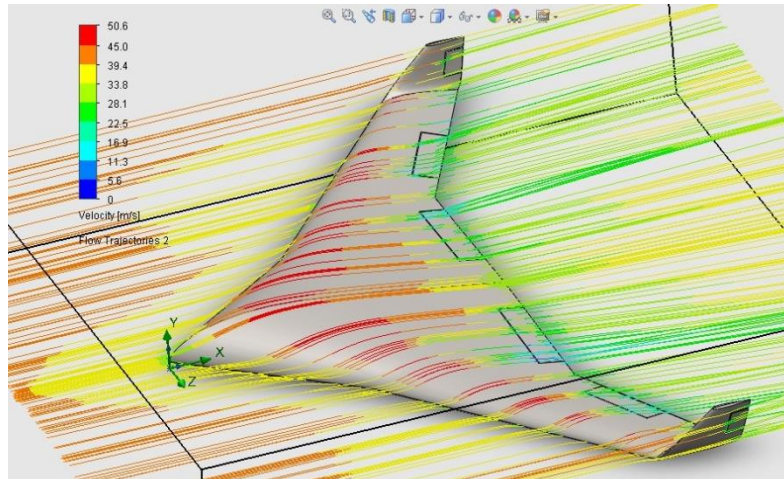
Figure 25

The CFD analysis on the cavity-closed structure showed no turbulence and a satisfying continuous flow.

These results led to the decision of closing the cavities on the structure by some sort of closing mechanism which was determined in the second semester.

14.2 Numerical analysis results:

After deciding to close the cavities, a numerical analysis of the preliminary performance was carried out using a cavity-closed structure model.

Using the data of the airfoil that was chosen (EPLER E334) and numerical models from the literature, a Matlab code was written and the following results were achieved:

UAV data:

Model top surface- $S = 0.918m^2$

Wing span- $b = 1.77m$

Weight- $W = 9.92lb = 4.5Kg$

Zero-lift drag coefficient- $C_{D_0} = 0.006$

Zero AOA lift coefficient- $C_{L_0} = 0.35$

Lift curve slope- $C_{L_\alpha} = 6.76\frac{1}{rad}$

Stalling AOA- $\alpha_{st} = 11.5^o$

Numerical model:

Environment conditions were assumed to be at sea level, due to the fact that the aircraft was design to cruise at very low altitude.

$$\rho_{SL} = 1.225\ \frac{Kg}{m^3}$$

$$T_{SL} = 288K$$

Some of the parameters were unknown and needed to be calculated.

Aspect ratio- $AR = \frac{b}{s^2} = 3.41$

Max lift coefficient- $C_{L_{Max}} = C_{L_0} + C_{L_\alpha} \cdot \alpha_{stall} = 1.71$

Oswald efficiency number- $e = 1.78 \cdot (1 - 0.44 \cdot AR^{0.68}) - 0.64 \approx 0.95$

Calculations coefficient- $k = \frac{1}{\pi \cdot AR \cdot e} \approx 0.1$

Reference surface- $S_{Ref} = \frac{S}{2} = 0.46m^2$

Wing loading - $\frac{W}{S} = 4.9\frac{Kg}{m^2}$

Level flight-

Dynamic pressure- $q = \frac{1}{2}\rho V^2$

Equations of motion:

$$T = D = qS\left(C_{D_0} + KC_L^2\right)$$

$$L = W = qSC_L$$

$$V = \sqrt{\frac{2}{\rho C_L}\left(\frac{W}{S}\right)}$$

Actual $\frac{T}{W}$:

$$\frac{T}{W} = \frac{1}{\frac{L}{D}} = \frac{qC_{D_0}}{\frac{W}{S}} + \left(\frac{W}{S}\right)\frac{K}{q}$$

Stalling velocity:

$$V_{stall} = \sqrt{\frac{2W}{\rho SC_{L_{max}}}} = \sqrt{\frac{2W}{\rho SC_{L_\alpha} \cdot \alpha_{stall}}} = 17.98\frac{m}{s} = 34.95 knots$$

Minimum thrust required for level flight:

When demanding $\frac{\partial D}{\partial V} = 0$:

Aerodynamic efficiency- $\frac{L}{D} = \left(\frac{L}{D}\right)_{max} = 20.36$

Cruise speed- $V_{minimum\ thrust\atop or\ drag} = V^* = \sqrt{\frac{2W}{\rho S}\sqrt{\frac{K}{C_{D_0}}}} = 24.93\frac{m}{s} = 48.46 knots$

Lift coefficient- $C_{L_{minimum\ thrust\atop or\ drag}} = C_L^* = \sqrt{\frac{C_{D_0}}{K}} = 0.2526$

Minimum drag or thrust- $D_{min} = T_{min} = qS\left[C_{D_0} + K \cdot \frac{C_{D_0}}{K}\right] = 2qSC_{D_0} = 2.17 Kgf$

Minimum power required for level flight:

Required power-

$$P_{req} = D \cdot V = qS\left(C_{D_0} + KC_L^2\right) \cdot V = \frac{1}{2}\rho V^3 S\left(C_{D_0} + KC_L^2\right) = \frac{1}{2}\rho V^3 SC_{D_0} + \frac{KW^2}{\frac{1}{2}\rho VS}\frac{\partial D}{\partial V} = 0$$

When demanding $\frac{\partial P_{req}}{\partial V} = 0$:

Cruise speed- $V_{minimum\ Power} = V^+ = \sqrt{\frac{2W}{\rho S}\sqrt{\frac{K}{3C_{D_0}}}} = 18.94\frac{m}{s} = 36.82\ knots$

Lift coefficient- $C_{L_{minimum\ Power}} = C_L^+ = \sqrt{\frac{3C_{D_0}}{K}} = 0.44$

Drag $- D_{minimum\ Power} = qS(C_{D_0} + 3C_{D_0}) = 2D_{min} = 4.34 Kgf$

Minimum required power- $P_{req} = 465.2 Watts$

Matlab code results:

Using a Matlab code, we were able to achieve the drag, power and aerodynamic efficiency diagrams at different cruise velocities of the aircraft:

Figure 26 presents the aircraft aerodynamic efficiency at different cruise velocities.
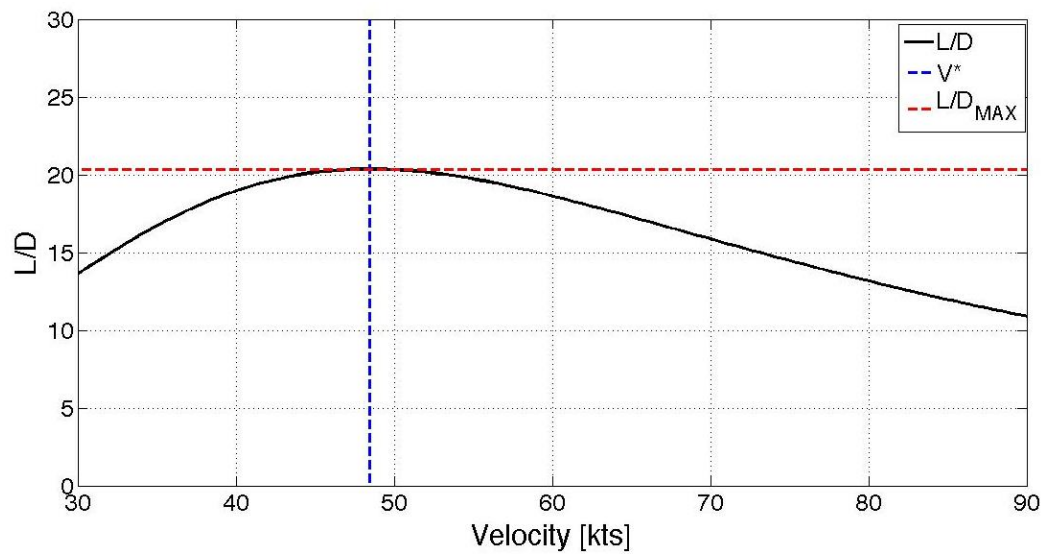

Figure 26

Shown in figure 26 is the calculated $\frac{L}{D}$ at different velocities. As mentioned before, the maximum of the curve is achieved at the speed for minimum drag (V^*), and its value ≈ 20.

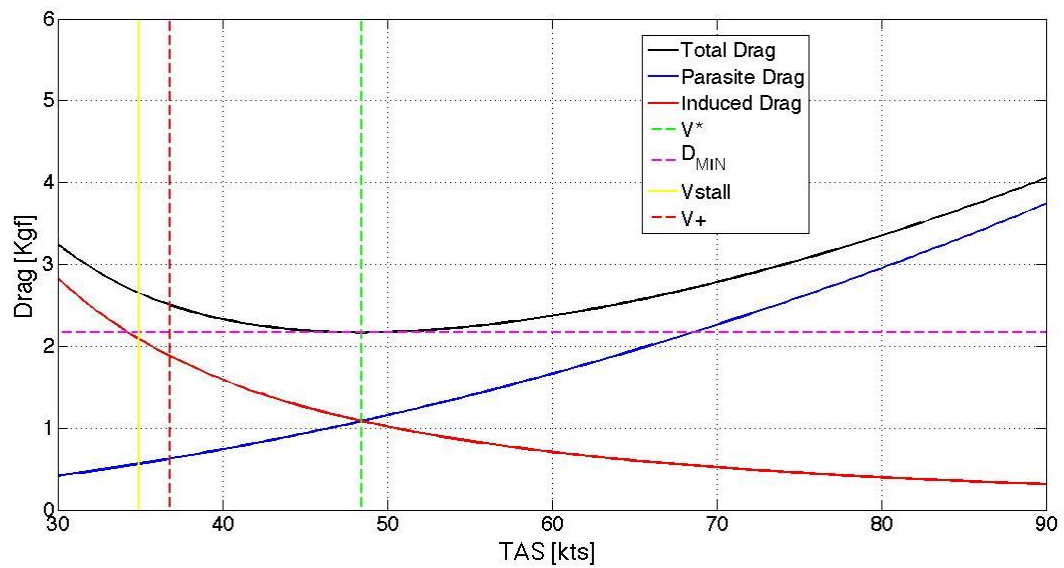Figure 27 presents the aircraft drag at different cruise velocities.

Figure 27

When examining the graph of the drag above, it was concluded that drag values between $V = 40 - 60 \, knots$ is very similar, and this is the range of velocities that at which the aircraft will be the affected by the drag.

The required power at different cruise velocities is presented in figure 28.
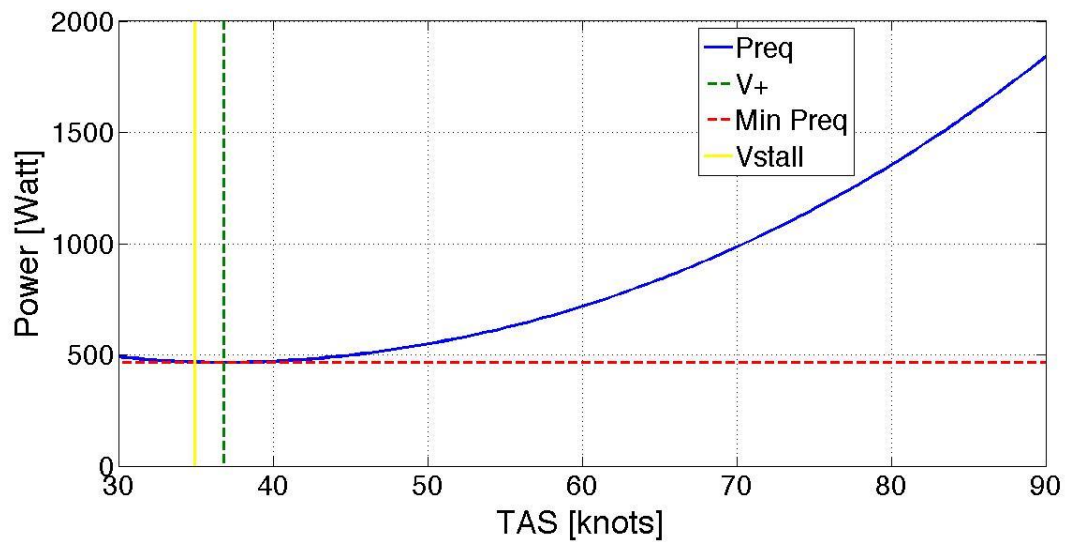

Figure 28

Figure 28 presents the required power for overcoming the drag. When choosing the cruise velocity for the aircraft, this graph is the most important due to the fact that the lower the required power will be during the cruise, the lower the weight of the engines' batteries will be to ensure the endurance needed.

35

The previous calculations showed that cruise velocity for minimum required power was $V^+ = 36.8$kts but when observing the results, higher velocity was chosen due to the small difference between the calculated velocity V^+ and the stalling velocity $V_{stall} \approx 35kts$.

The cruising velocity was than chosen to be $\approx V^* \approx 48knots$, the required power was calculated- $P_{req} \approx 530Watts$.

Endurance performances:

The batteries for the vertical flight were chosen to work for 2 minutes during the take-off and the landing (each part- 2 minutes) , a reasonable time for the vertical motors to lift the UAV to a minimum height in which the horizontal motor will start working and complete the take-off, and a good time for landing due to fact that less thrust is needed during the landing.

 The batteries for the horizontal flight were chosen to work for 20 minutes and supply a maximum value of 700 Watts (take-off) to the engine at all times. After examining the results from the numerical analysis, it was concluded that the batteries can achieve this endurance and more, due to the lower power that was required during the cruise.
Horizontal endurance – 4 minutes.
Vertical endurance $\approx$ 20 minutes.

Range performances:

Vertical range – $R = V_{cruise} \cdot t_{endurence} = 30Km = 18.64\ miles$.

Maneuvering performances – V-n diagram:

Maximum load factor was assumed to be – $n_{max} \approx 3.8$
Corner Speed- speed of turns – $V_A = 67.1kts$
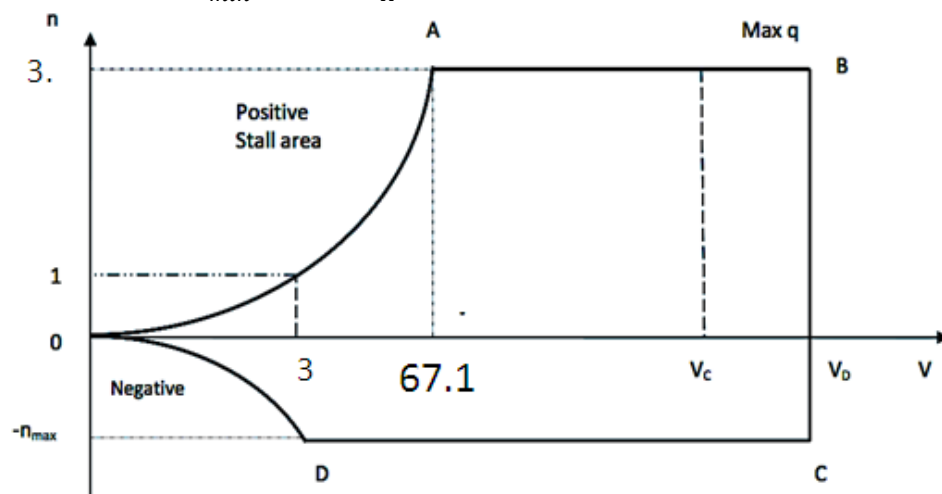Minimum turn radius – $R_{min} = 33m\ ; V_A$

Figure 29

Maximum turn rate – $\dot{\psi} = 1.04\frac{m}{s}; V_A$
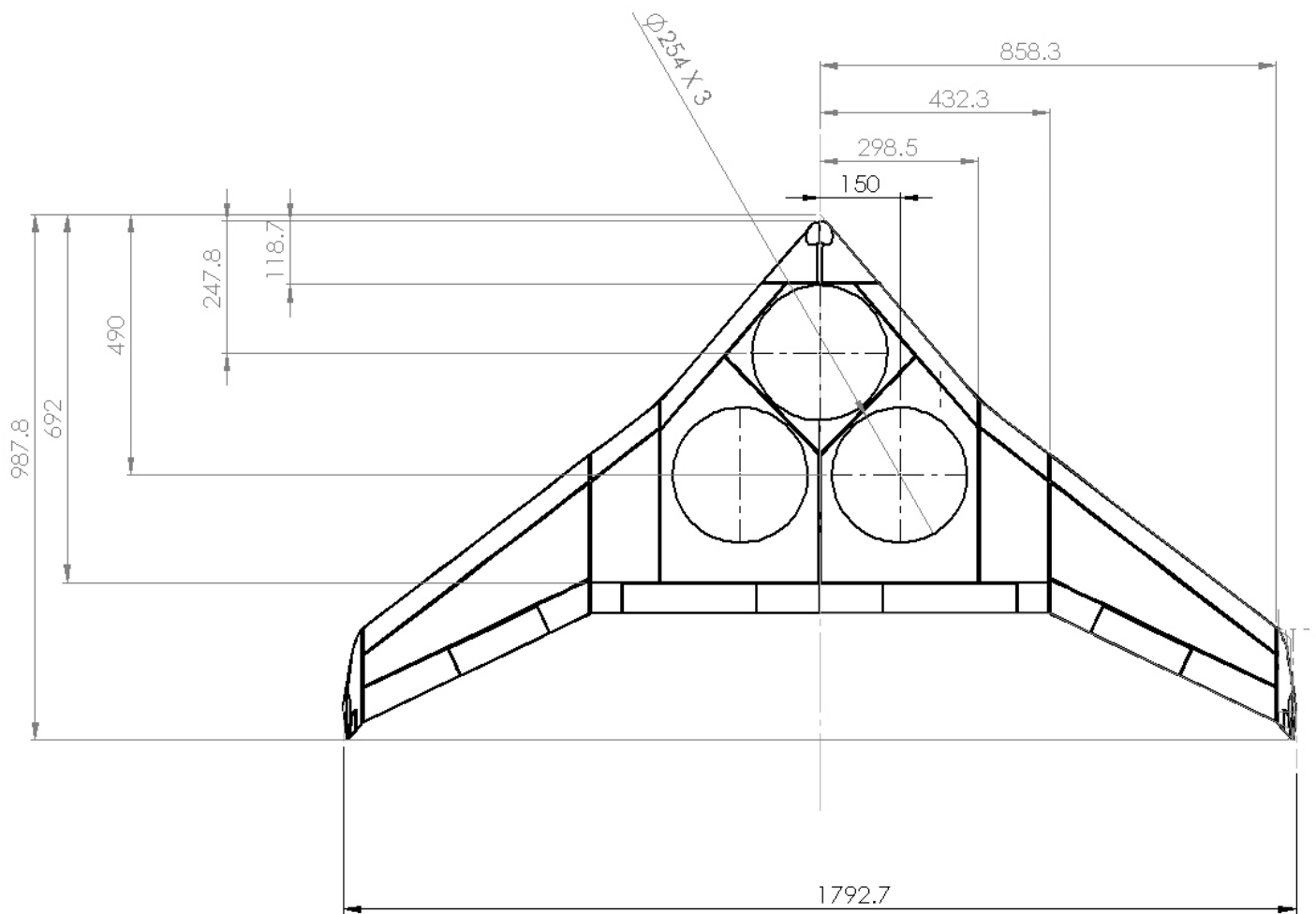
15. Plan form and dimensions

Figure 30

16. Systems installation arrangement (Internal Lay-Out)

Components:

5. 1 payload
6. 3 vertical motors
7. 1 horizontal motor
8. 4 electronic speed controllers
9. 3 Batteries
10. 1 autopilot

The first installation principle was accessibility since it is critical to verify that all inner components are accessible for maintenance. The second installation principle was weight and balance. In order to maintain stability it is crucial to keep the center of gravity (C.G) before the aerodynamic center. Therefore, the components are installed so that the C.G in place.

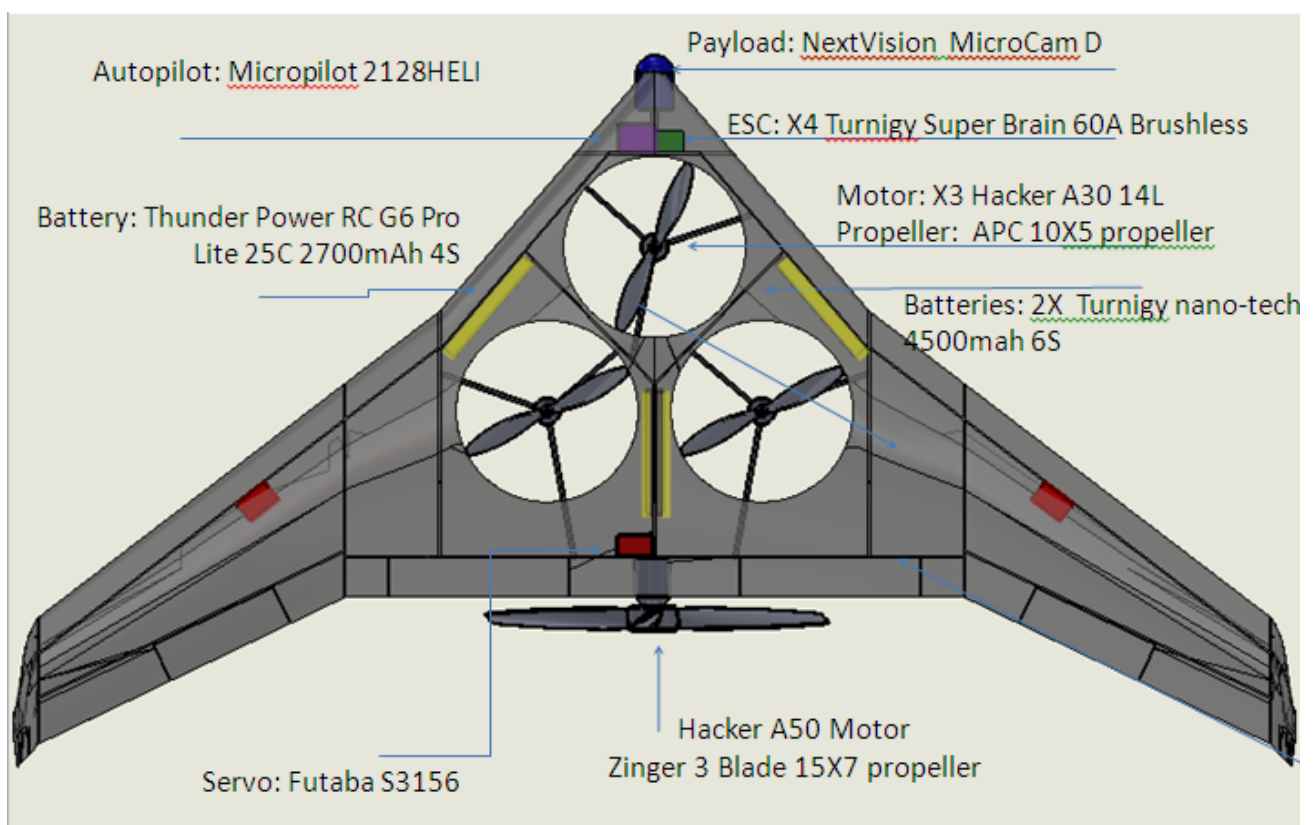Figure 31 presents the system installation arrangement.

Figure 31

17. Conceptual design of wing structure

The wing structure was based on leading edge spars, trailing edge spars, ribs and mid-fuselage reinforcement (figure 32).
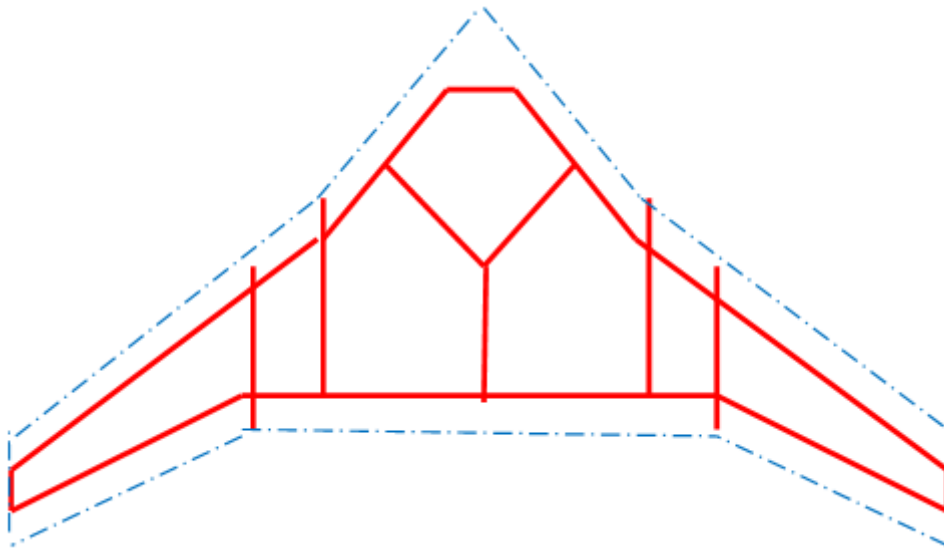

Figure 32

On top of the spars and reinforcement was placed a thin Kevlar skin, as seen in figure 33.
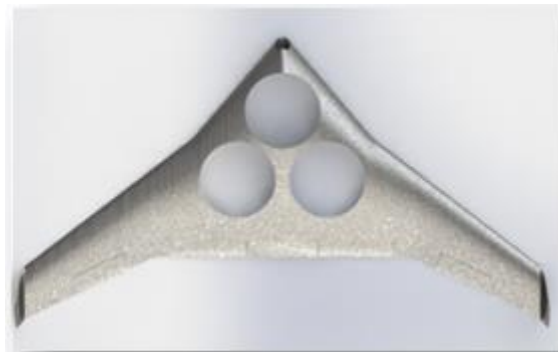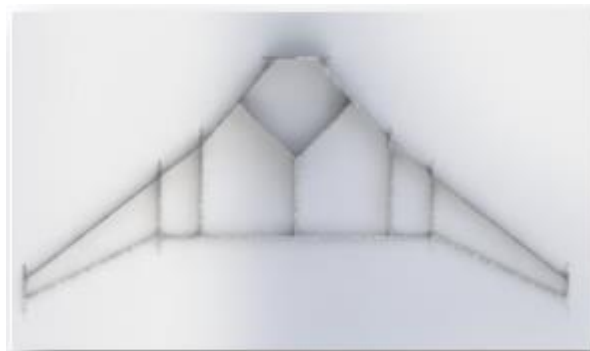

Figure 33

Figure 34

18. Detailed design of outer wing

A detailed design of the outer wing was made (figure 35).

Figure 35

Initial assumptions and data:

- Work under bending load.

- Wing area is 0.09[m^2]

- The 0.45[m] span wing is subject to 2.25[kg] force.

- Wing load is 25[Kg/m^2].

- Under 3.8G (Normal category) the wing load equals to 95[Kg/m^2].

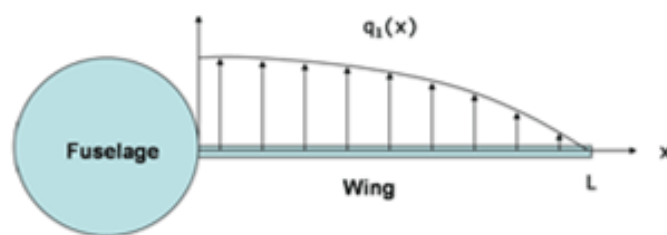The wing is modeled as a beam, as shown in figure 36.

Figure 36

The lift acts as a bending force over the wing, therefore a reinforcement is needed. As accepted in aviation, this reinforcement comes as a main beam or spar along the wing.

Our wing has 2 Spars and 2 ribs: One main spar and one trailing edge spar, and tip and root ribs

Figure 37
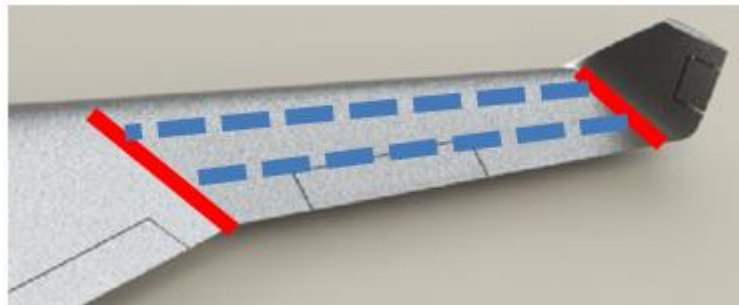
Figure 38

The next step is designing the cross-section of the spar.

In order to resist bending force, High moment of inertia is needed. It can be done by rectangular cross-section as shown in the following figure, but weight is a major factor and it can be reduced by an I beam.

Although I beam is satisfying solution, U beam can produce better performance as easier manufacturing.
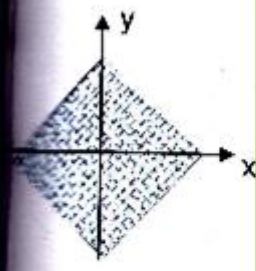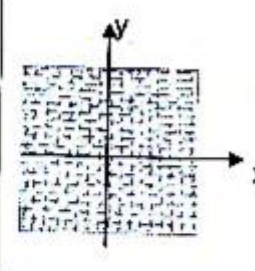
Figure 39

Web and flange material:

- Carbon Fabric (45deg)

Flange support:

- Carbon unidirectional (UD)

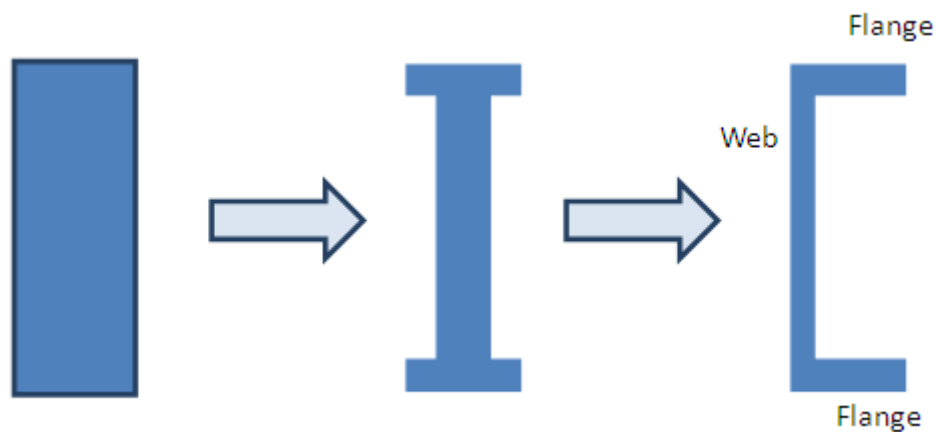| Carbon Fabric		Carbon UD	תאור
45°	0-90°	U.D.	
$E_X = E_Y = 1200$	$E_X = E_Y = 6000$	12000	$E = \left[Kg/mm^2\right]$
$G_{XY} = 3000$	600 -300	600 -300	$G = \left[Kg/mm^2\right]$
$\tau_{XY} = 6$	$\sigma_X = \sigma_Y = 6$	$\sigma = 120$	חוזק
	$\tau_{XY} = 6$		Kg/mm^2 לשבר
$\gamma = 2000\ \mu S$	$E = 1000\ \mu S$	$E = 10000\ \mu S$	התארכות לשבר

Figure 40

Spar dimensions:

ž   Main spar:

ž
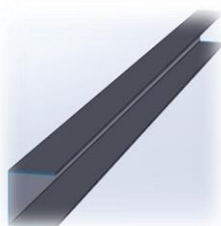
- Web height – forced by wing geometry

- Flange Width– Calculated by bending load analysis under the assumption of constant thickness of 1mm
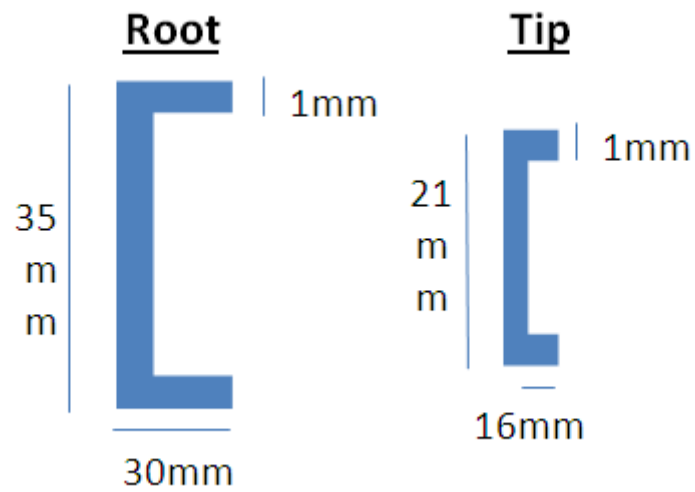
Figure 41

ž **Trailing edge spar:**
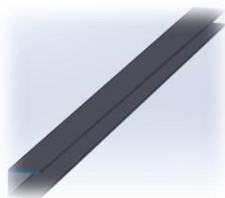
ž

ž Web height – forced by wing geometry

ž Flange Width– Designed for smooth operation of the aileron control system
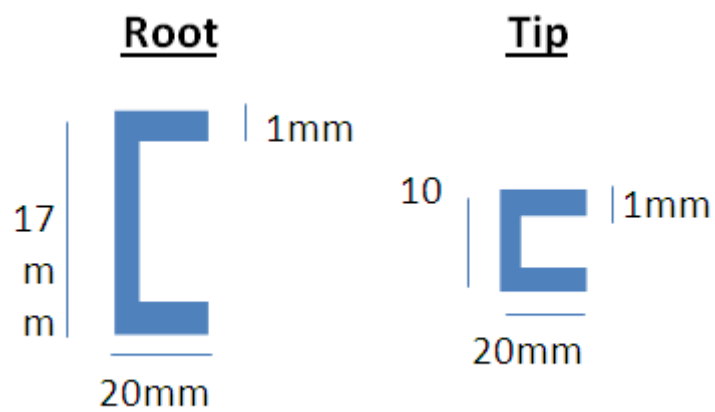
Figure 42

Spars location:

Main spar is located at 25% chord.

Trailing edge spar is parallel to the ailerons hinges line, using for support aileron hinges.
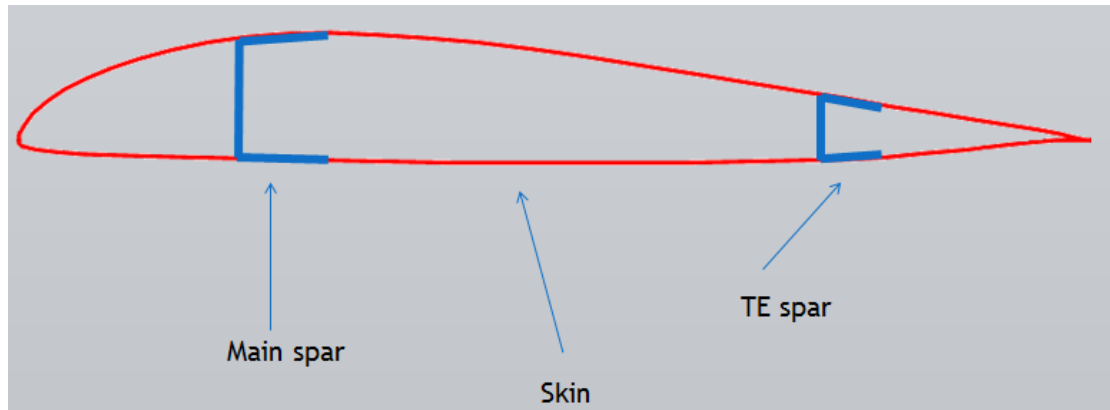
Aileron control system

To minimize drag, ailerons control system is located inside the wing.
The aileron is connected to the trailing edge spar by a piano hinge at the upper surface and by control rod at the lower surface.

Movement of the aileron controlled by a servo located in the inside the wing space, attached to the trailing edge spar, as shown in the following figure.
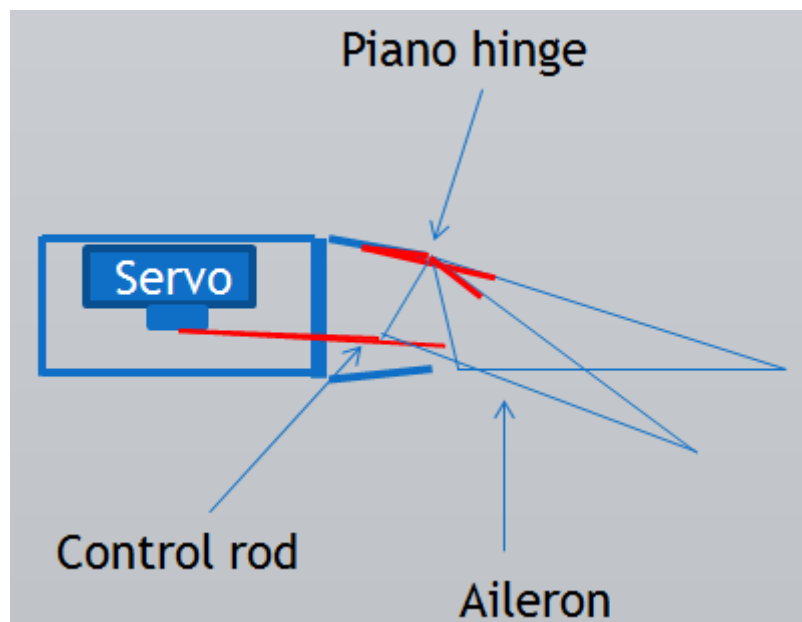
The chosen aileron servo is the Futaba S3156MG.
It has been chosen due to its high torque, low weight and high reliability.

S3156 Micro		
FUTM0656		
Volts	**Torque**	**Speed**
4.8V	28 oz-in (2.0 kg-cm)	0.13 sec/60°
6.0V	33 oz-in (2.4 kg-cm)	0.11 sec/60°
Dimensions		**Weight**
7/8 x 7/16 x 7/8 in. (22 x 11 x 22 mm)		0.33 oz (9.3 g)
		3P, BB, MG

Figure 45

Root and tip ribs

- EPPLER 334 airfoil shaped

- Tip is made of 1mm carbon fabric

    - Holes for electrical wires

    - Connection to the winglets

Figure 46

- Root is made of 3mm carbon fabric

    - Holes for electrical wires

    - Supports the outer wing spars

Figure 47

Figure 48

45
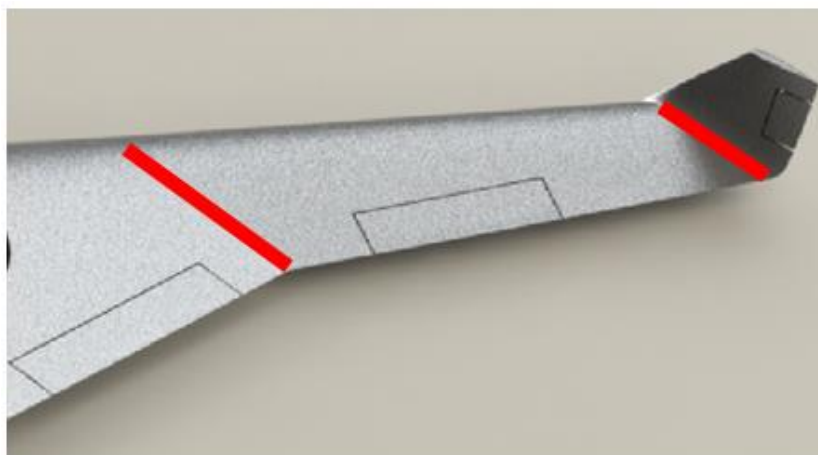
Connection to the main body
is made by two spars and one pin:

Figure 49

Tip rib

Main spar

Root rib

Trailing edge
spar

Figure 50

46
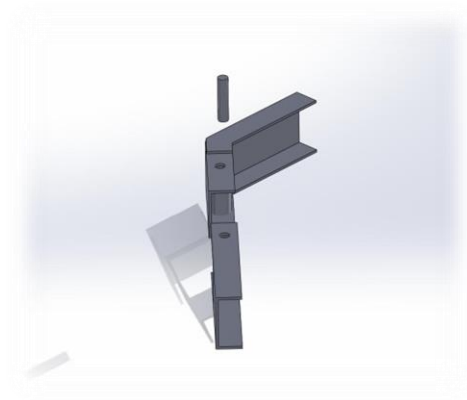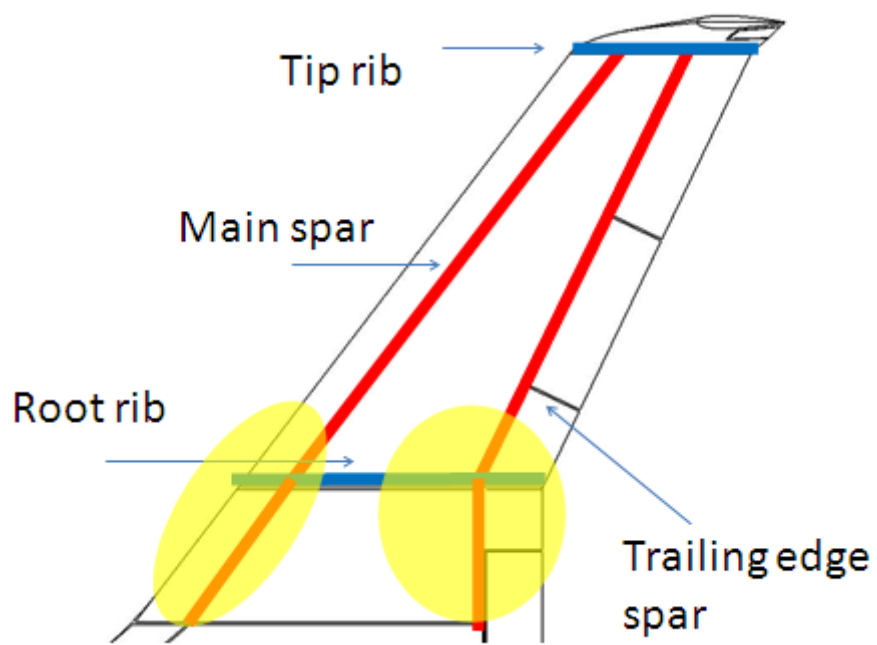
19. Rotors cavity closing mechanism

As seen in the preliminary performance analysis, it is necessary to close the cavities of the rotors in order to maintain satisfying performances of the UAV. Two different closing mechanisms were investigated: the Shutters mechanism and the Iris mechanism.

A detailed design was made for each mechanism and with SolidWorks program it was attempted to attach the mechanisms to the UAV. Both were designed to cover a 10 inches cavity and to enable opening and closing of the cavity.

The investigated mechanisms are presented ahead.

19.1 Shutters mechanism:

The first mechanism that was investigated was the shutters mechanism, which is a simple mechanism, used in houses.

The shutters mechanism is comprised of a ring to which the shutters are connected with poles. The end of each pole is bended and connected to a wire that rounds the ring from the outside (figure 51).
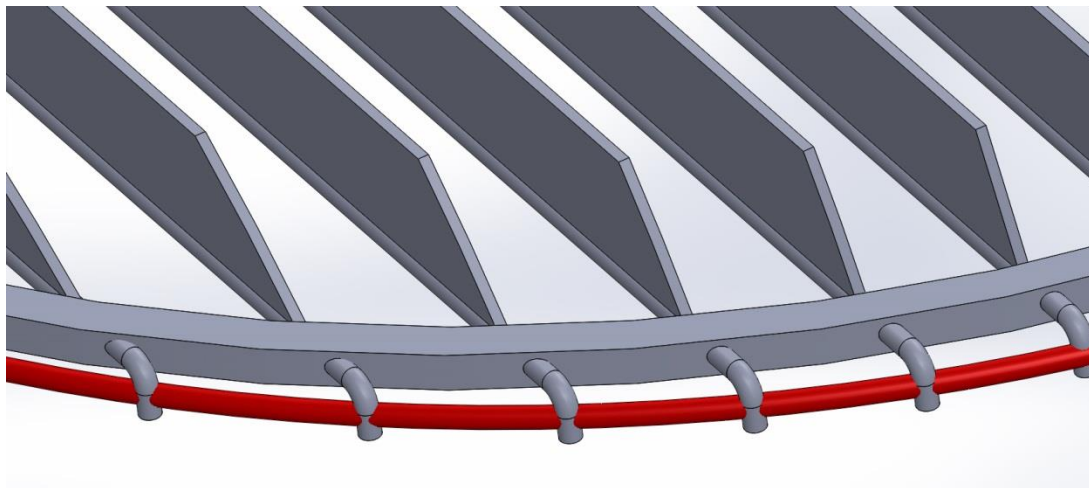
Figure 51

The designed mechanism is presented in figure 52. The inner diameter of the ring is 10 inches which is the diameter of the vertical propeller that was chosen. The outer diameter of the ring is 10.4 inches and the ring's thickness is 5 mm. the shutter's height is 13 mm each and their thickness is 1 mm each. When the shutters are opened, the total height of the mechanism is about 10 mm. the cable's diameter is 2 mm.
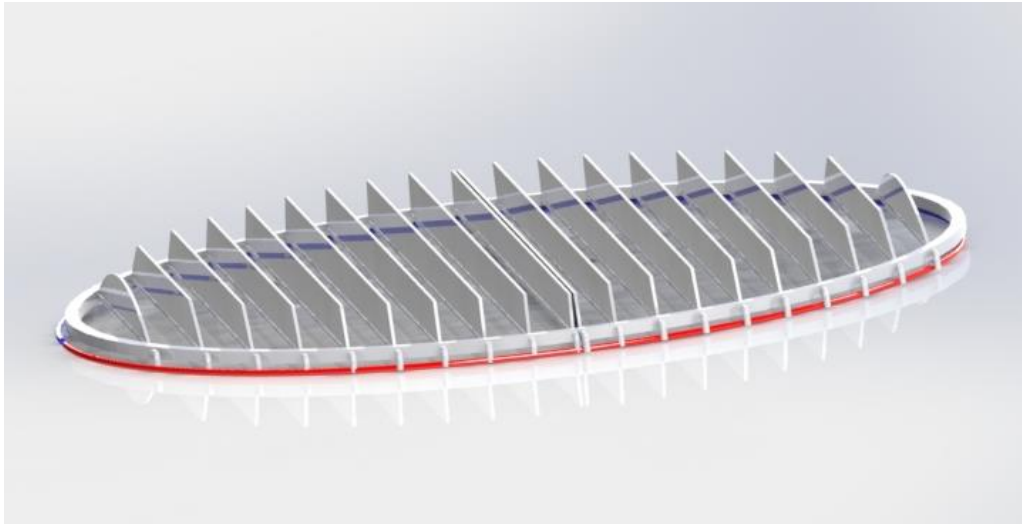
Figure 52

Figure 53 presents the mechanism closing process. On the top right corner is the fully opened mechanism wile on the bottom is the fully closed mechanism. On the top left corner is the half closed mechanism.
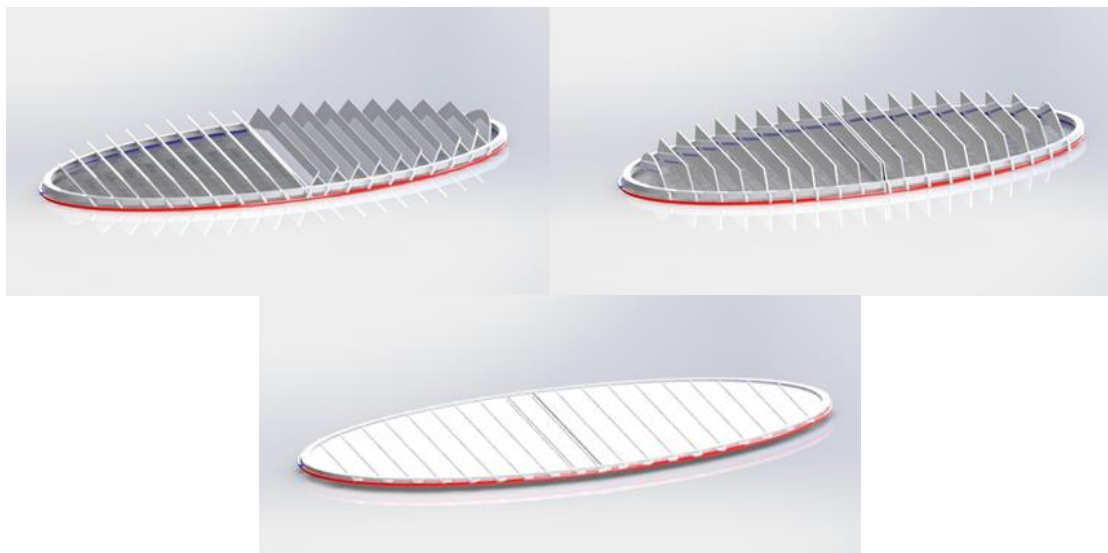
Figure 53

A study of the shutters mechanism has raised several advantages. The first and most crucial is the small outer diameter of the ring which complies with the maximal diameter allowed under the UAV's limitations. Another advantage is the simplicity of the mechanism as well as its low height in closed configuration. However, during vertical take-off and landing the opened shutters may interrupt the flow and affect the UAV's performance.

19.2 Iris mechanism:

Another mechanism we investigated was the Iris mechanism which is a simple shutter, used mainly in cameras, and enables to close a round hole with ease.

The Iris is comprised of two rings mounted on each other, one stationary and one that can rotate. Between the rings are segments that open and close with the rotation of the top ring (figure 54).
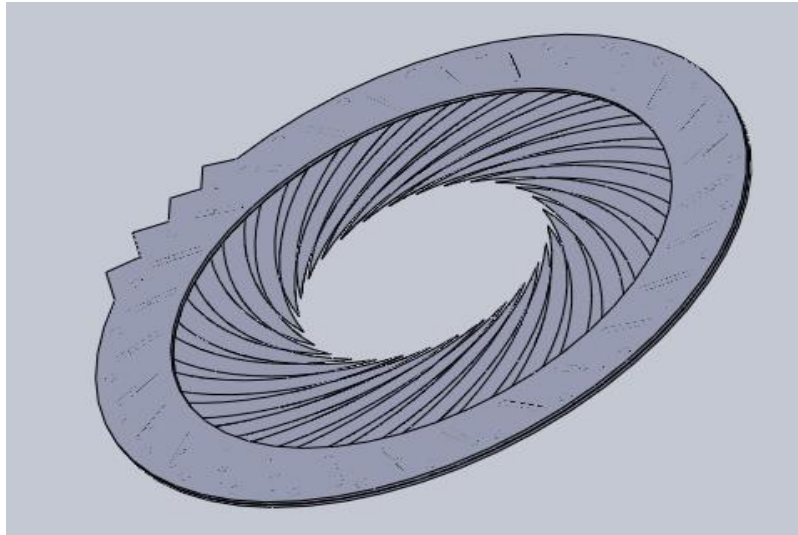
Figure 54

Figures 55 to 57 show the designed mechanism. The outer diameter is 13 inches while the inner diameter is 10 inches which is the diameter of the propeller that was chosen. The thickness of the top and base ring is 2 mm. In total, there are 28 Segments positioned with a small angle of 5 degrees. The thickness of each segment is 0.2 mm. When the iris opens 5 segments are overlapping which brings the total thickness to 5 mm.

Figures 55 and 56 present the segments and the rings of the mechanism, respectively. On the left of figure 56 is the base ring while on the right is the rotating ring.

Figure 55

49
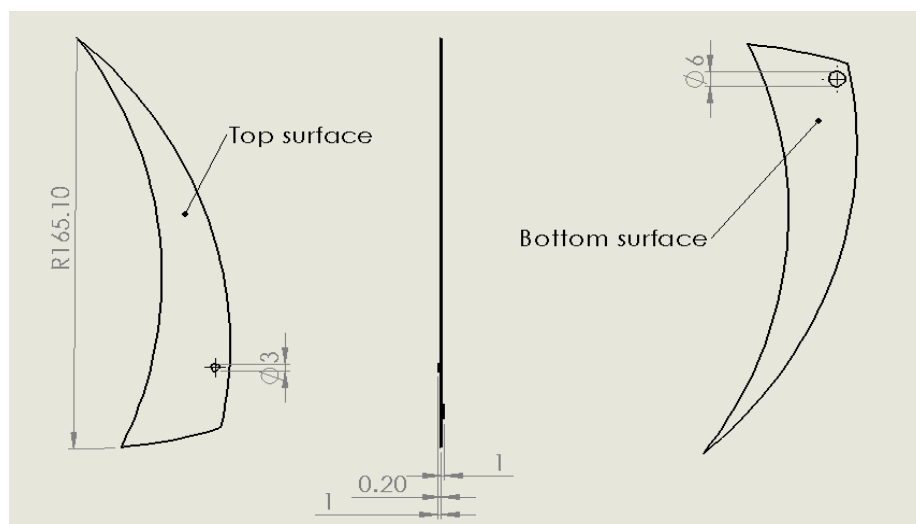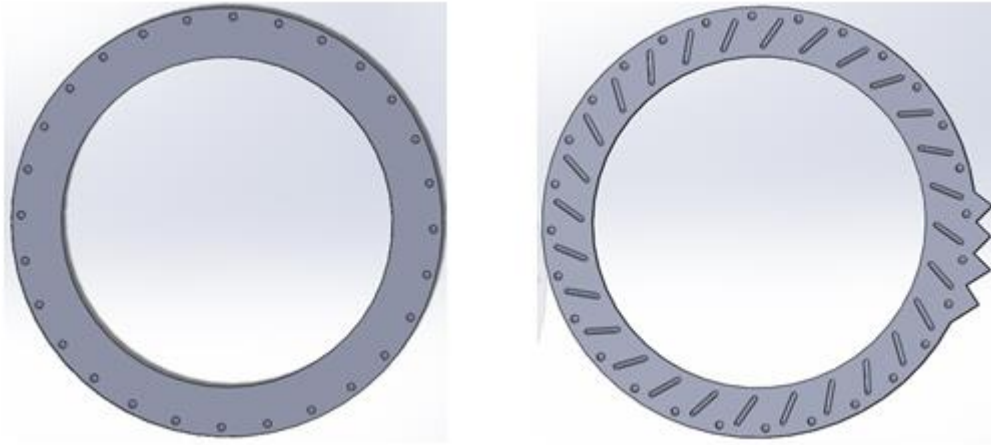
Figure 57 shows the mechanism's closing process. On the top left corner is the closed mechanism while at the bottom is the opened mechanism. On the top right corner is the half closed mechanism. It can be seen that the top ring rotates to close the segments.

Closed iris

Half opened iris -
Top ring rotates

Opened iris
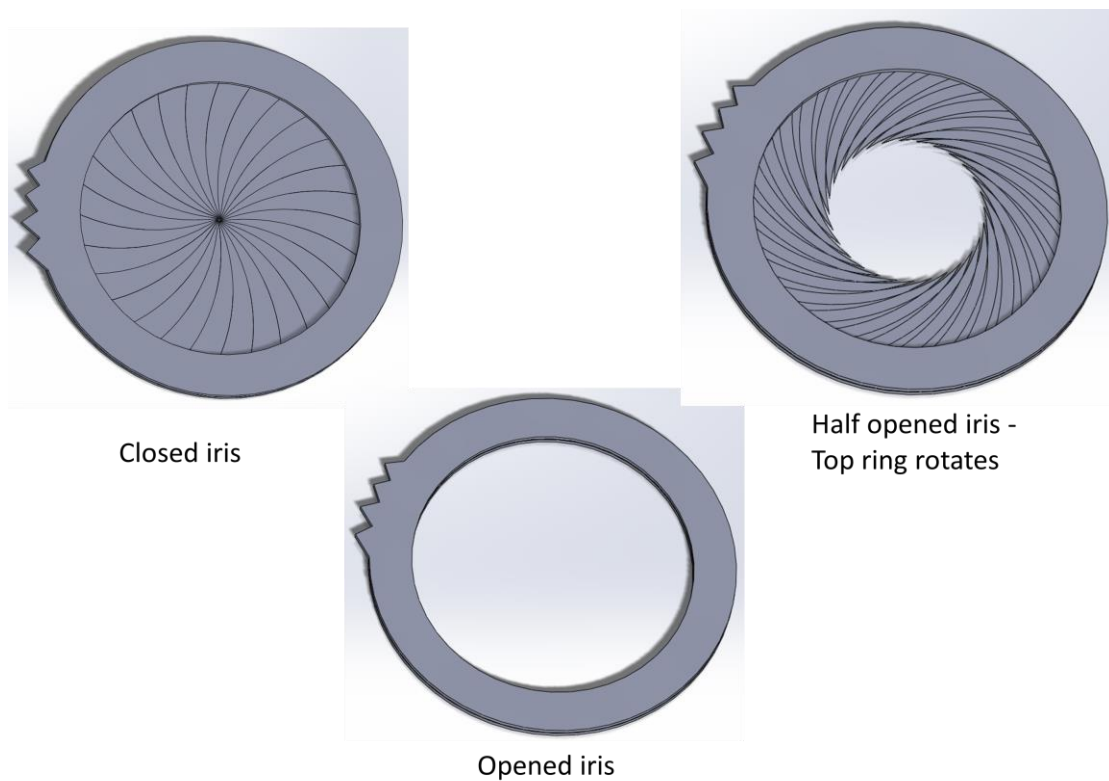
After studying the Iris mechanism, several advantages were found. The first was that it does not impair the air flow when the hole is fully opened. Another advantage is the simple design which can be operated easily with a small servo. Moreover, during vertical take-off and landing the mechanism will not interrupt the flow.

On the other hand, the UAV has limited space and the Iris mechanism requires a diameter larger than the one allowed. Reduction of the outer diameter is dependent of additional

segments which will cause friction and inability to open or close the system. Furthermore, since the curved design of the UAV does not comply with the contour of the Iris mechanism, craters will appear in the body and will affect the UAV's performance.

The closing mechanism must have a minimal outer diameter in order to fit into the UAV. Furthermore, the thickness of the mechanism must be as thin as possible since the UAV has limited space in it. Due to these considerations, the chosen mechanism was the shutters which can be installed on top of the UAV rather than in it.

20. Control system

Due to the unique design of the UAV, it was decided to use two different control systems: A tri-rotor system to control the ascent and descent altitude and a more common control system to control the level flight.

The UAV's control system requires:

- Inertial Sensors:
    - Linear and angular accelerometers
    - Gyroscopes
- Air Data Sensors:
    - Flow direction (α,β)
    - Flight speed sensor (Pitot)
    - Altimeter
- Optic sensors, GPS, etc.

All of the above are included in the chosen controller, Micropilot 2128HELI.

20.1 Tri-Rotor modeling

The basic tri-rotor UAV configuration (figure 58) is two parallel rotors with opposite rotation. There is also a single tilted rotor in order to counter the reaction torque of the system. This allows the tilt angle α to enable all three degrees of freedom motion as well as hovering.
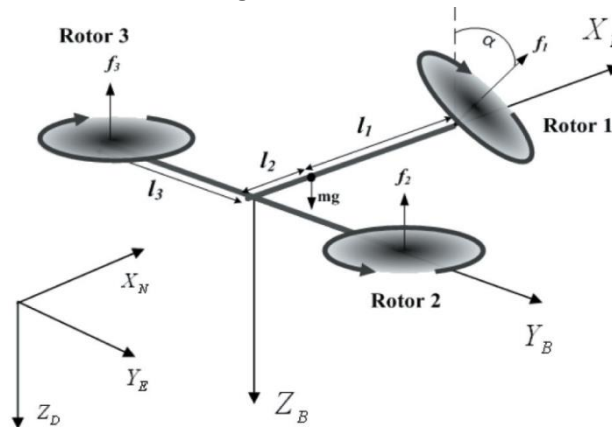
The force and moment equations for this configuration are the following:

$$\bar{F} = \begin{bmatrix} 0 \\ f_1 \sin\alpha \\ -f_2 - f_3 - f_1 \cos\alpha \end{bmatrix}$$

$$\overline{M} = \begin{bmatrix} -l_3(f_2 - f_3) \\ -l_2(f_2 + f_3) + l_1 f_1 \cos\alpha \\ l_1 f_1 \sin\alpha - \tau_1 \cos\alpha + \tau_2 - \tau_3 \end{bmatrix}$$

The four motion controls for this model are altitude, yaw, pitch and roll. All movements are available through a change in α or through the angular velocity Ω:
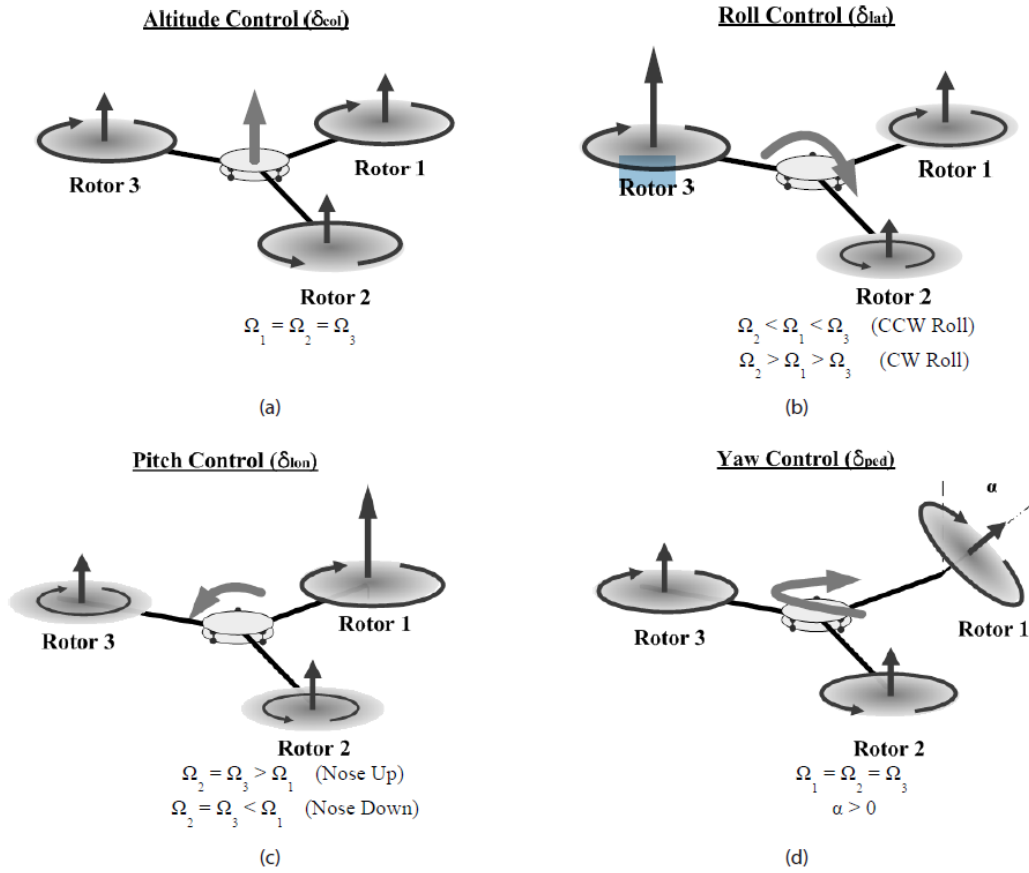
Figure 59

Since the tri-rotor model is used only for altitude control, it is most important to position all three rotors on the same plane and providing them with the same angular velocity. This will enable steady take-off and landing.

The movement equation than becomes very simple:

$$m\ddot{z} = f_1 + f_2 + f_3 - mg$$
$$f_i = k_t \cdot \Omega_i^2$$

Where k_t represents the thrust coefficient of the rotor.

However, although the tri-rotor is used for take-off and landing only, the process has to be controlled in order to reduce interferences which may cause the UAV to deviate.

In order to maintain a steady parallel take-off and landing, there is a need to control the attitude of the three rotors. It is needed to keep them synched and to allow them to compensate for interferences by providing each motor a specific velocity.

To maintain a steady take-off and landing with compensation for interference, attitude hold autopilot modeling (figure 61) was used. The attitude hold autopilot tracks the pitch, roll, and yaw angles and holds them. It consists of a double loop, while the inner-loop represents angular-rate feedback and the outer-loop represents attitude feedback.
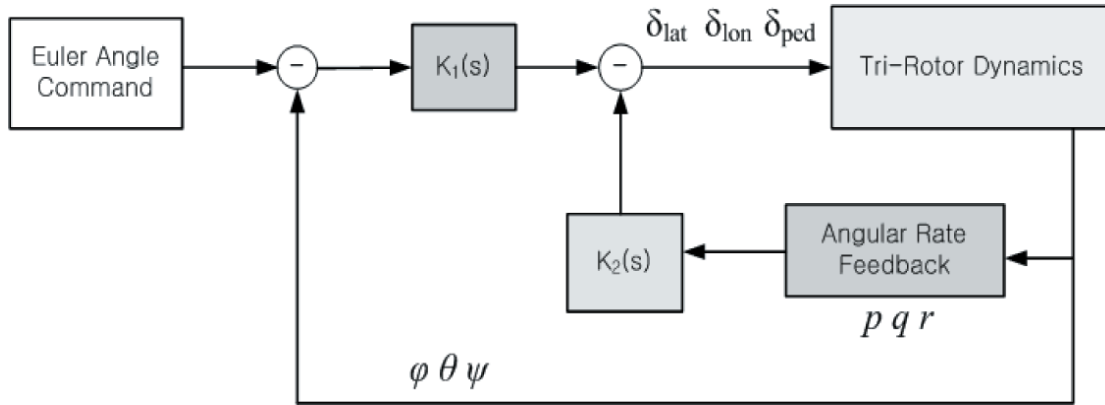
Figure 60

20.2 Flight Transition

During the flight there are two transition steps. The first is the transition from vertical take-off to level flight. The second transition is from level flight to vertical landing.

In order to control the transition, the block diagram showed in figure 62 was used. This system controls the tri-rotor execution with altimeter feedback in order to identify the moment in which the UAV has reached the desired altitude. Then, the system sends a command for the horizontal motor and for the flight speed control to reach the desired flight speed. In the same time, it shuts down the vertical motors and also closes the shutters. The Pitot feedback notifies the system when it has reached the desired flight speed.

Figure 61

20.3 Level Flight Control

The aspiration was to model UAV and build a transmission equation to represent it.

The linear modeling of the lateral dynamics equations:

$$
\begin{Bmatrix} \dot{\beta} \\ \dot{p} \\ \dot{r} \\ \dot{\phi} \end{Bmatrix} = \begin{bmatrix} Y_v & 0 & -1 & g/U_0 \\ L'_\beta & L'_p & L'_r & 0 \\ N'_\beta & N'_p & N'_r & 0 \\ 0 & 1 & 0 & 0 \end{bmatrix} \begin{Bmatrix} \beta \\ p \\ r \\ \phi \end{Bmatrix}
$$

$$
+ \begin{bmatrix} Y^*_{\delta_a} & Y^*_{\delta_r} \\ L'_{\delta_a} & L'_{\delta_r} \\ N'_{\delta_a} & N'_{\delta_r} \\ 0 & 0 \end{bmatrix} \begin{Bmatrix} \delta_a \\ \delta_r \end{Bmatrix} - \begin{bmatrix} Y_v \\ L'_\beta \\ N'_\beta \\ 0 \end{bmatrix} \beta_g
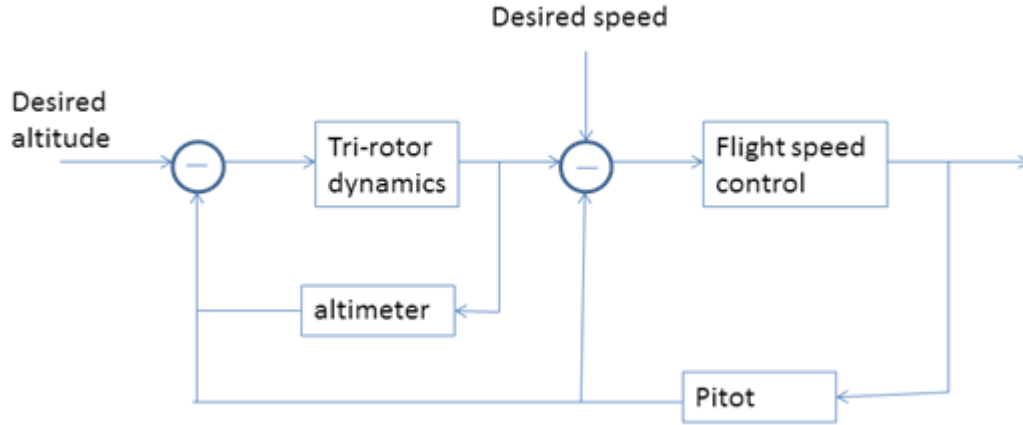$$

$$
\dot{\psi} = r
$$
$$
\dot{y} = U_0(\beta + \psi)
$$
$$
a^{meas}_{y_{cg}} = U_0(\dot{\beta} + r) - g\phi
$$

The linear model of the longitudinal dynamics:

$$
\begin{Bmatrix} \dot{u} \\ \dot{w} \\ \dot{q} \\ \dot{\theta} \end{Bmatrix} = \begin{bmatrix} X_u & X_w & 0 & -g \\ Z_u & Z_w & U_0 & 0 \\ \bar{M}_u & \bar{M}_w & \bar{M}_q & 0 \\ 0 & 0 & 1 & 0 \end{bmatrix} \begin{Bmatrix} u \\ w \\ q \\ \theta \end{Bmatrix} + \begin{bmatrix} X_{\delta_e} & T_{\delta_T} \\ Z_{\delta_e} & 0 \\ \bar{M}_{\delta_e} & 0 \\ 0 & 0 \end{bmatrix} \begin{Bmatrix} \delta_e \\ \delta_T \end{Bmatrix} - \begin{bmatrix} X_u & X_w \\ Z_u & Z_w \\ \bar{M}_u & \bar{M}_w \\ 0 & 0 \end{bmatrix} \begin{Bmatrix} u_g \\ w_g \end{Bmatrix}
$$

The forces operating on the UAV are shown in figure 62.
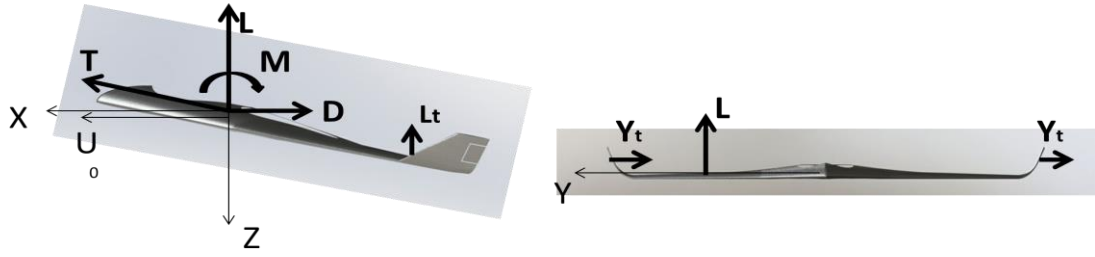
Figure 62

Using the linear modeling it was attempted to model the UAV. However, the equations require 34 different coefficients which are derived from experiments such as tunnel test experiment and forces analysis.

The tunnel test yielded only a quarter of the required coefficients. This prevented expressing the UAV as a transmission equation and performing profound control analysis. Therefore, only the basic block diagram for the control system can be presented. Given the plane dynamics, the UAV can be fully expressed as a mathematical equation.

20.3.1 Pitch Angle Control Diagram
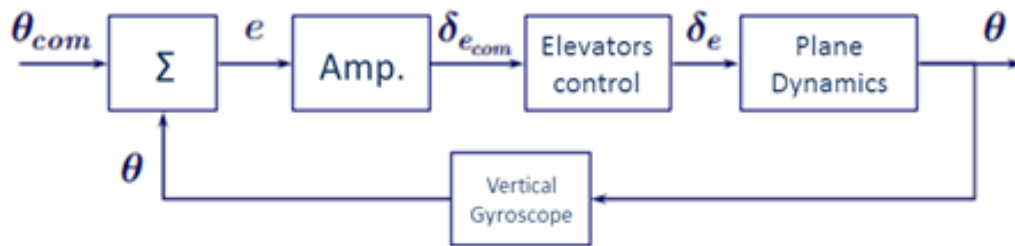
Figure 63

20.3.2 Automated Lateral Flight

The basic diagram for automated pilot with elevators and rudders control is shown in figure 64.

Figure 64

56
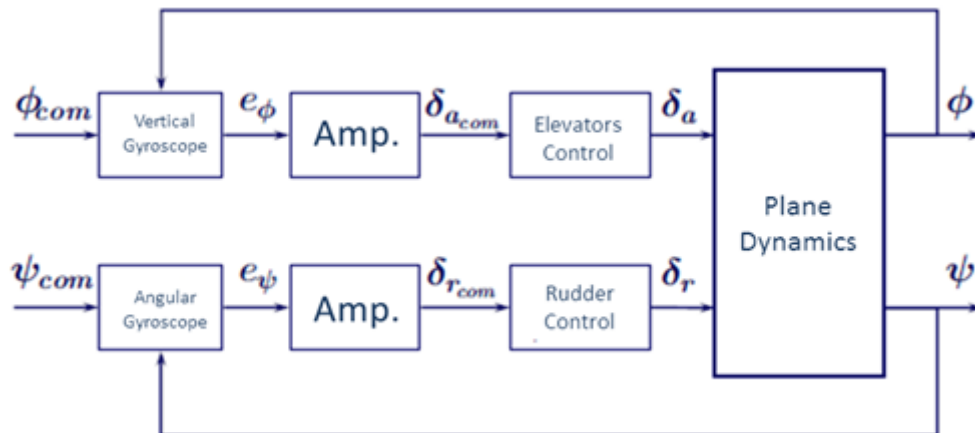
20.3.3 Turn Coordination

1. *β control with angle feedback*
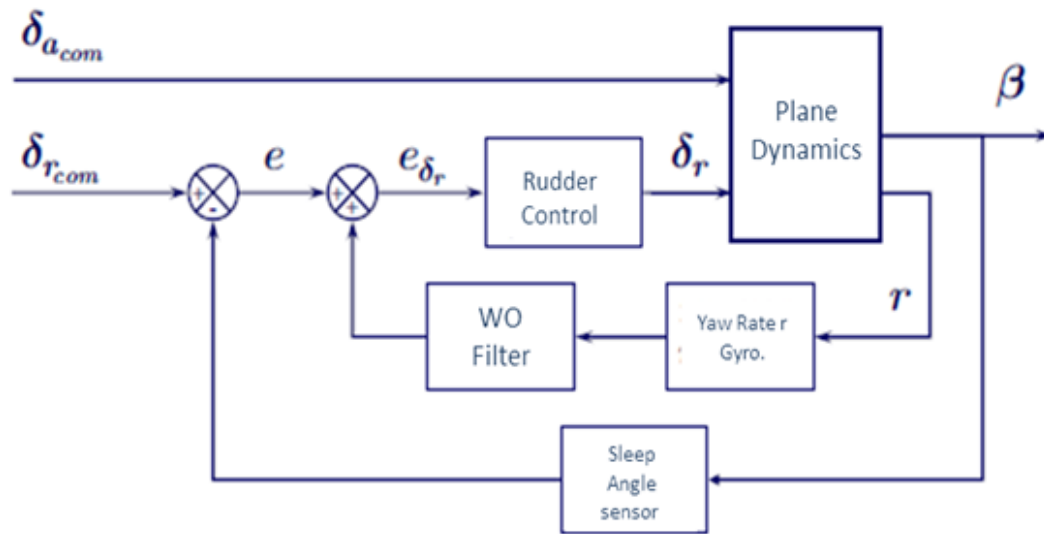
Figure 65

2. *α control with lateral acceleration feedback*

Figure 66

57
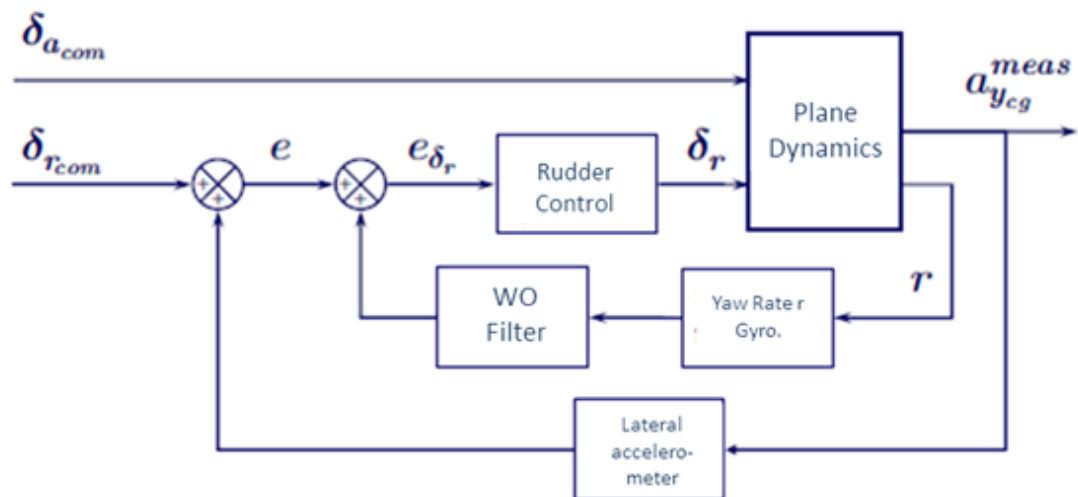
3. *Rudder Control*
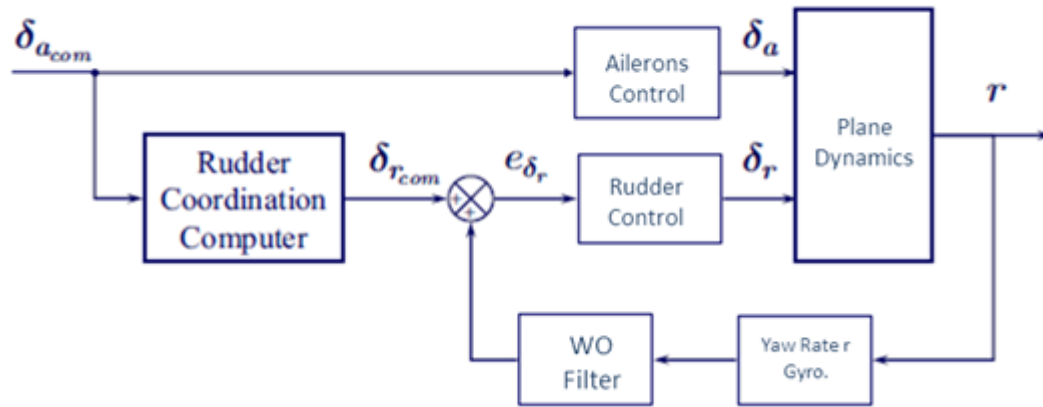
Figure 67

20.3.4 Yaw Rate Control

Figure 68 presents the basic diagram of yaw rate control in a coordinated plane.
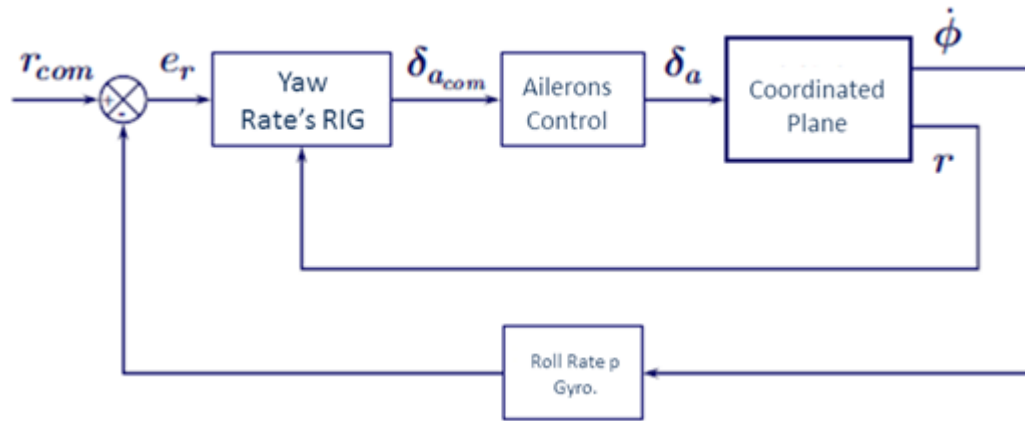
Figure 68

20.3.5 Roll Angle Control

Figure 69 presents the basic diagram of roll angle control in a coordinated plane.
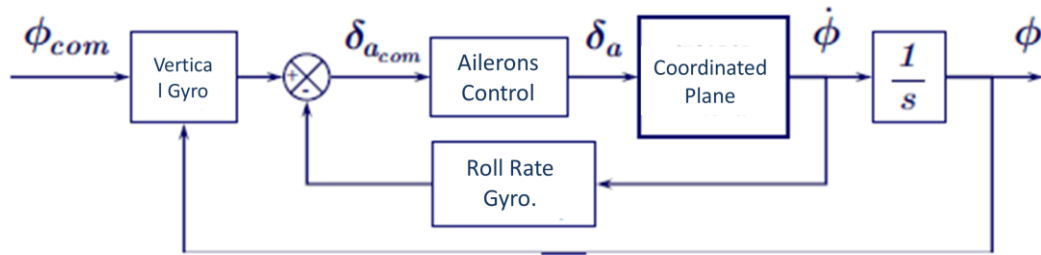
Figure 69

20.3.6 Flight Direction Control
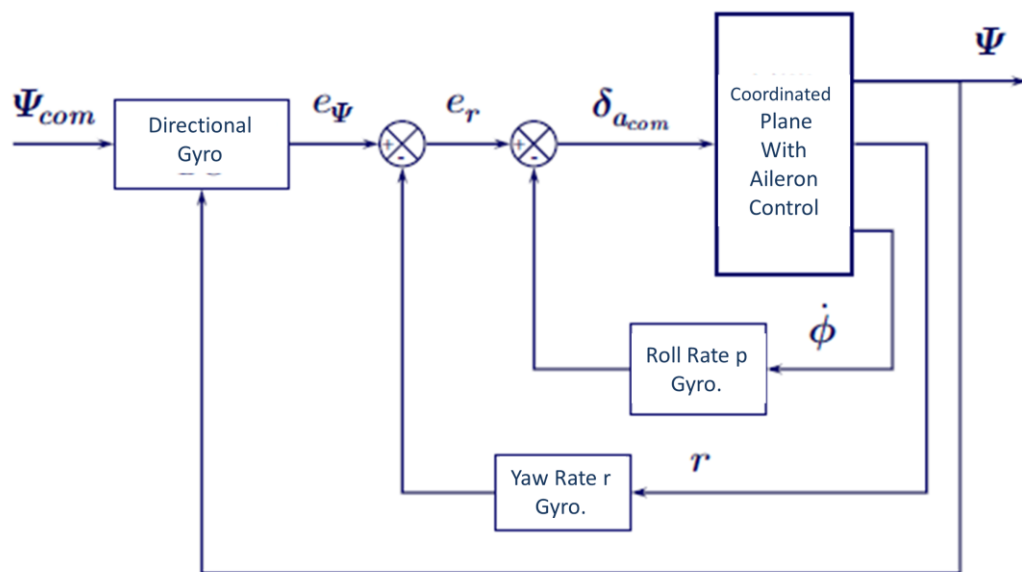
Figure 70

20.4 Flight Pattern

Figure 50 describes the flight pattern for the UAV, showing approximated times for each step. The pattern shows that at the beginning only the vertical motors are started and that after take-off the horizontal motor is started. Moreover, once the cruise speed has been reached, the vertical motors shut down. The opposite transition takes place at the end of the flight when the vertical motors shut down after landing.
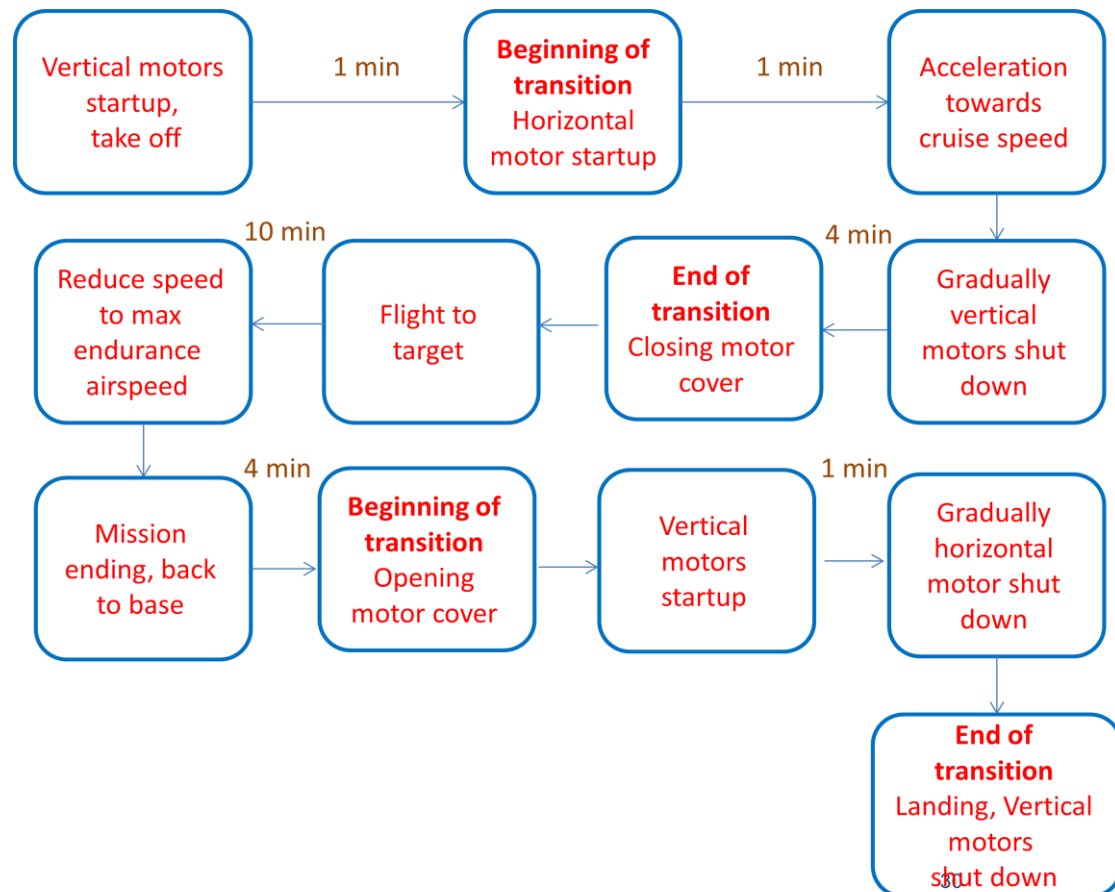
Figure 71

21. Weight and balance

The reference datum was specified as the payload.

Station	Weight [Kg]	Arm [m]	Moment [Kg*m]
Fuselage	1.1	0.822	0.653
Motor V1	0.143	0.26	0.039
Motor V2	0.143	0.55	0.083
Motor V3	0.143	0.55	0.083
Motor H4	0.43	0.77	0.331
Battery 1	0.67	0.1	0.053
Battery 2	0.67	0.1	0.053
Battery 3	0.72	0.387	0.108
Controller 1	0.03	0.107	0.003

Table 15

MTOW is 4.5Kg

C.G is located at 390mm
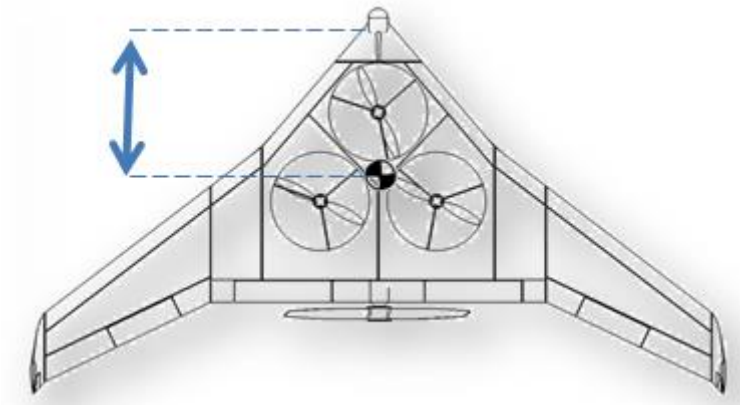
Figure 72

For positive stability margin, center of gravity had to be ahead of the pressure and aerodynamic center.

Figure 73 presents calculation using geometric method for swept and complex wing.
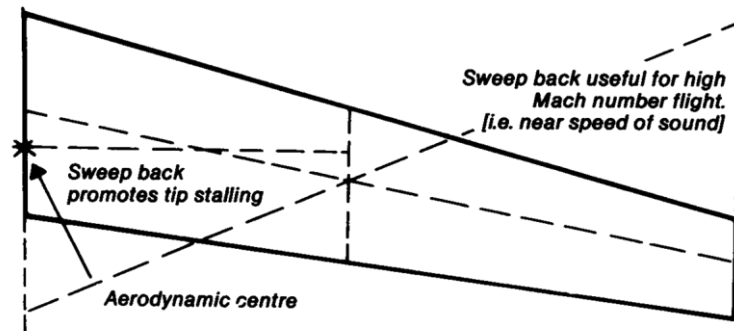
Figure 73

The flying wing shape was divided into rectangular, two trapezoids and one triangle. By summarizing the MAC of each part, the total MAC was received at 505mm from the reference datum.
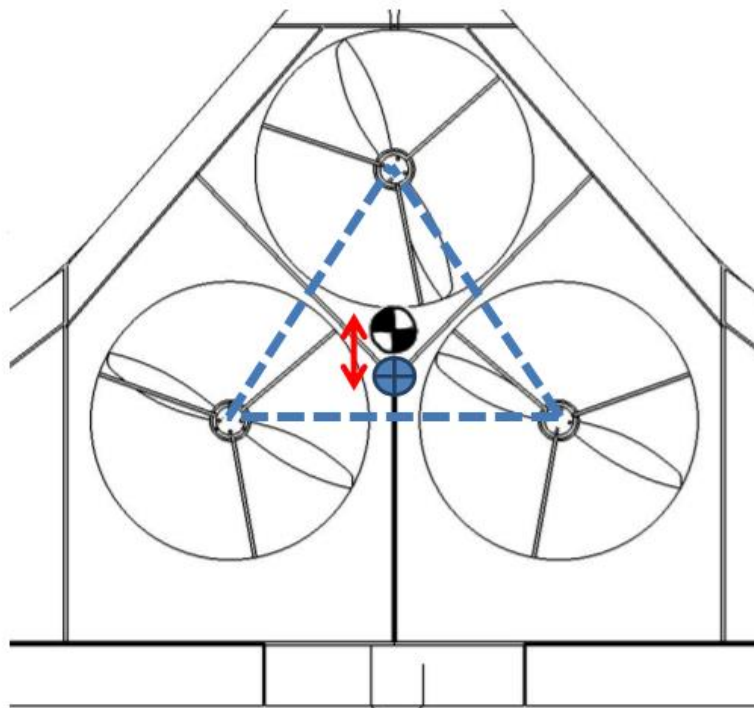
Figure 74

In order to enable vertical take-off and landing, the center of gravity must be exactly at the geometric center between the three motors.

22. Wind tunnel Test

A wind tunnel test was carried out in the Aerospace faculty wind tunnel.

22.1 Test purposes

The main purposes of the wind tunnel were:

- Verifying the predicted performances.
- Examining the option of leaving some of the cavities of the structures.
- Investigating the performances when leaving the cavities.
- Comparing rudders and splitter ailerons for yaw.
- Finding the aerodynamic center.

22.2 Model design

The chosen scale for the model was 1:2.5 due to the wind tunnel dimensions of 1x1 [m] and maximum blockage percentage of 4%.

A modification has to be done in the model in order to connect it properly to the mount of the tunnel. A cylindrical hole was created from the mid-fuselage backwards and small 'hill' was created above its center. The addition is presented in the following captures from SolidWorks:
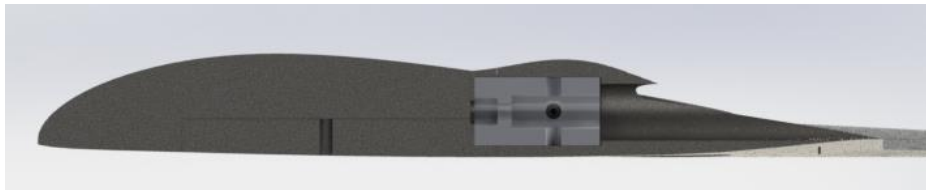
Figure 75
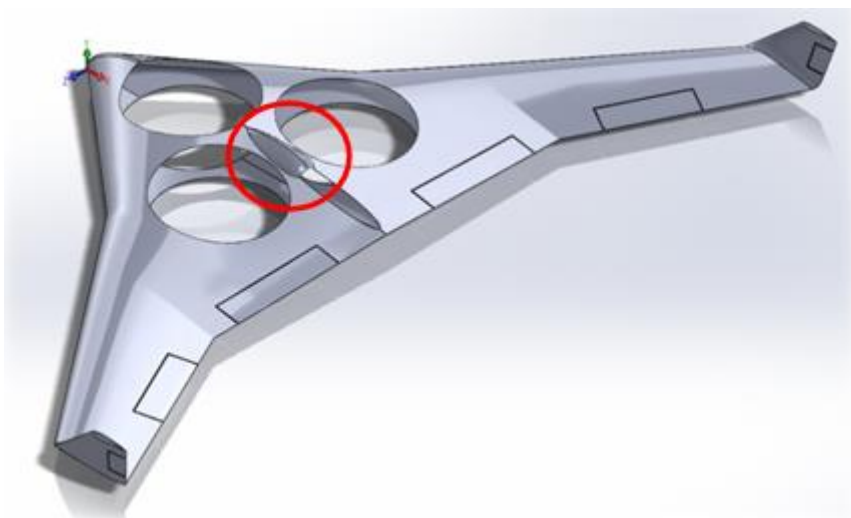
Figure 76

22.3 Manufacture process

The wind tunnel model was manufactured by rapid prototyping (3D print) and can be seen in figure 77.

The adapter and wing connection plate were manufactured by milling of aluminum.
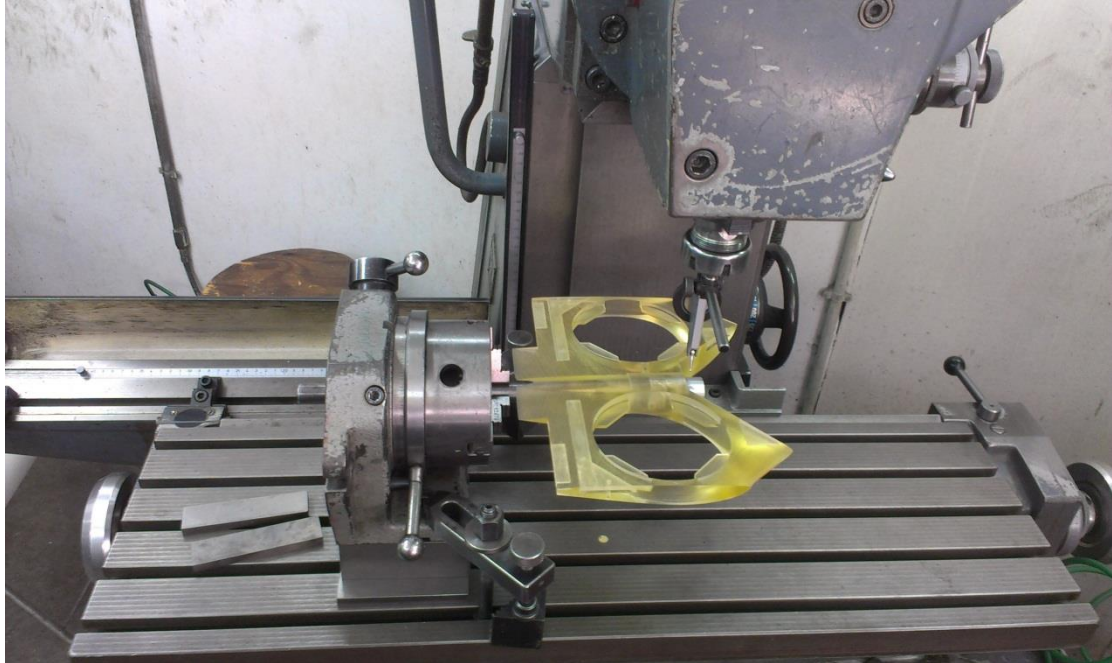
Figure 77

Due to the dimensions of the Objet260 printer, which are 260x260mm, it was necessary to split the fuselage into 4 parts: front, main, right and left wing (figure 78).

Figure 78

In addition, each vertical motor cavity is covered by removable upper and lower covers (figure 79).
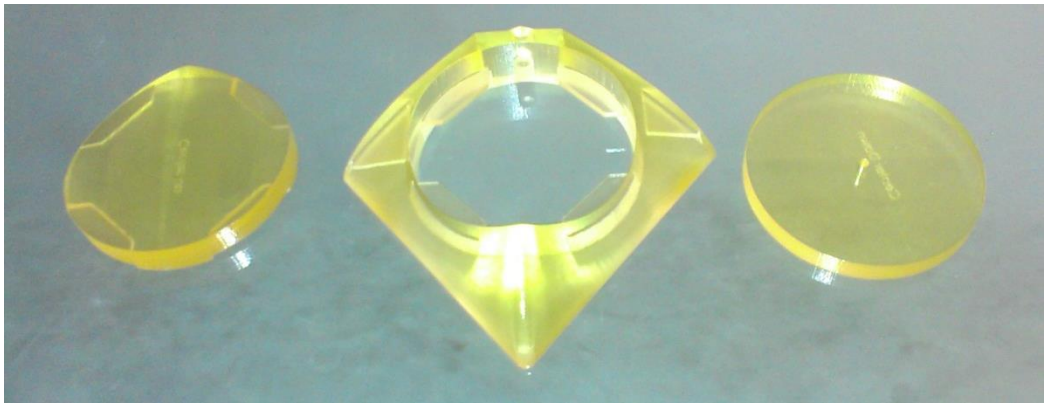
Figure 79

Each control surface (Aileron, Elevator, Rudder) has multiple variations as shown in table 16.

Ailerons [deg]	Elevator [deg]	Rudder [deg]	Split aileron[deg]
15	15	10	-15
7.5	7.5	5	
0	0	0	
-7.5	-7.5	-5	
-15	-15	-10	

16 Table

Overall, the model included 45 parts as shown in figure 80.
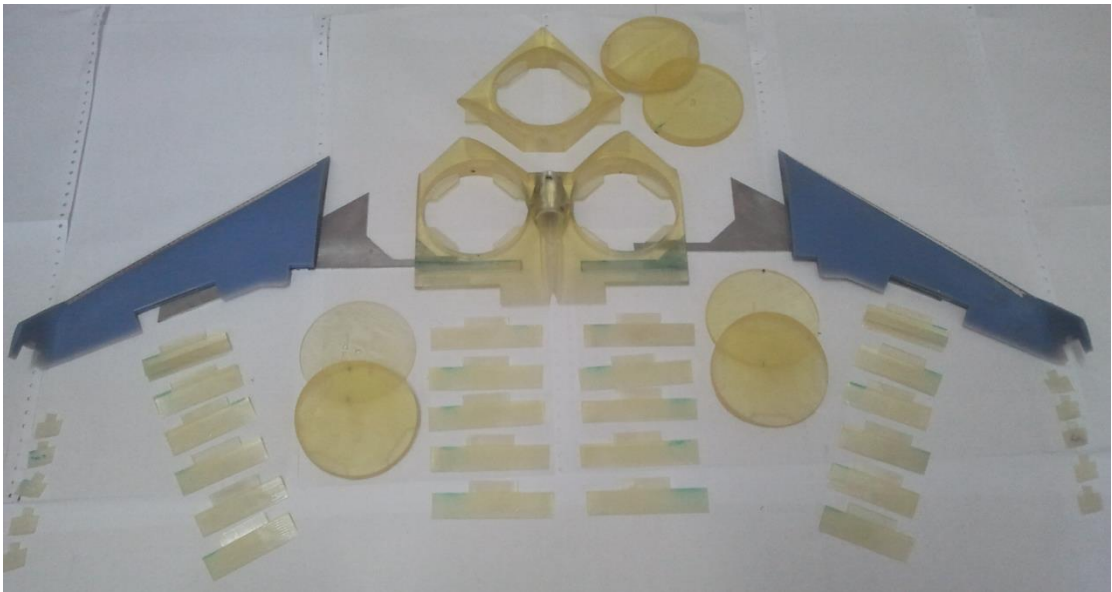
Figure 80

22.4 Test Outline

- Calibration run- verifying stalling AOA and determining running speed
- Closed cavities aircraft configuration:
    - Change elevators
    - Change ailerons including split aileron
    - Change rudders
- Top covers only configuration:
    - Change elevators
    - Change ailerons
    - Change rudders
- No covers configuration:
    - Change elevators
    - Change ailerons
    - Change rudders

The wind tunnel test plan is presented in the appendix chapter.

23. Wind tunnel test results evaluation

Prior to the wind tunnel test an initial assessment for the aircraft performance was carried out. The wind tunnel was made in order to verify the results of the preliminary analysis and to complete any gaps for information needed.

The analysis was made using a method that was taken from the literature and a Matlab code that were presented on the Preliminary performances chapter.

23.1 Calibration run

When designing the model for the wind tunnel test, a scale of 1:2.5 was chosen for tunnel limits reasons. In order to simulate real flight conditions, the conditions of the experiment have to keep the Reynolds number in the same range. One of the preliminary performance analysis conclusions was the cruise speed of the UAV, which was chosen to be $\approx 25\frac{m}{s} = 48kts$.

Reynolds number during real flight- $2 \cdot 10^5 < Re < 3 \cdot 10^5$. In order to keep the Reynolds number in this range, the air speed of tunnel has to be -$45\frac{m}{s} < V < 67\frac{m}{s}$.

Figure 81 presents the calibration run for $V = 35\frac{m}{s}$.
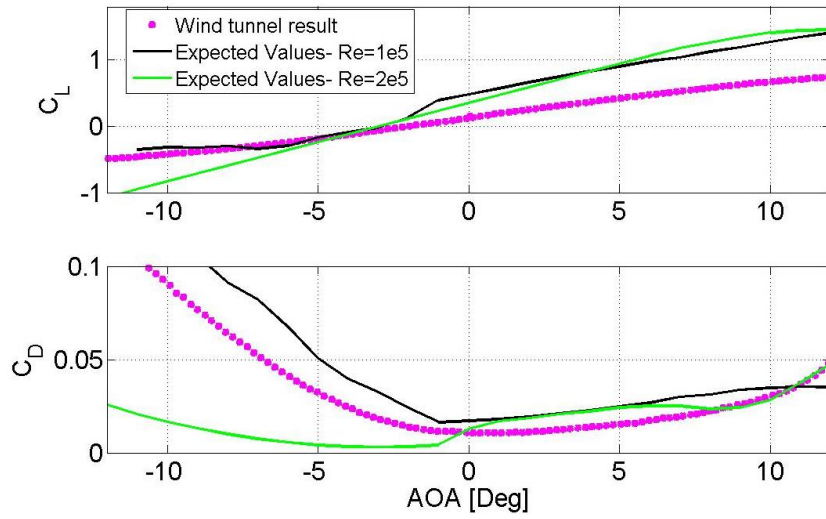
Figure 81

The first run was at tunnel speed- $V = 35\frac{m}{s}$ and different values of AOA. Vibrations on the model were noticed at $\alpha \approx \pm 12^O$ as expected. The lift and drag coefficients did not match the expected values of the airfoil at $Re = 2 \cdot 10^5$. When comparing the results to airfoil expected data at $Re = 1 \cdot 10^5$, better match was achieved.

Figure 82 presents the calibration run for $V = 45\frac{m}{s}$.
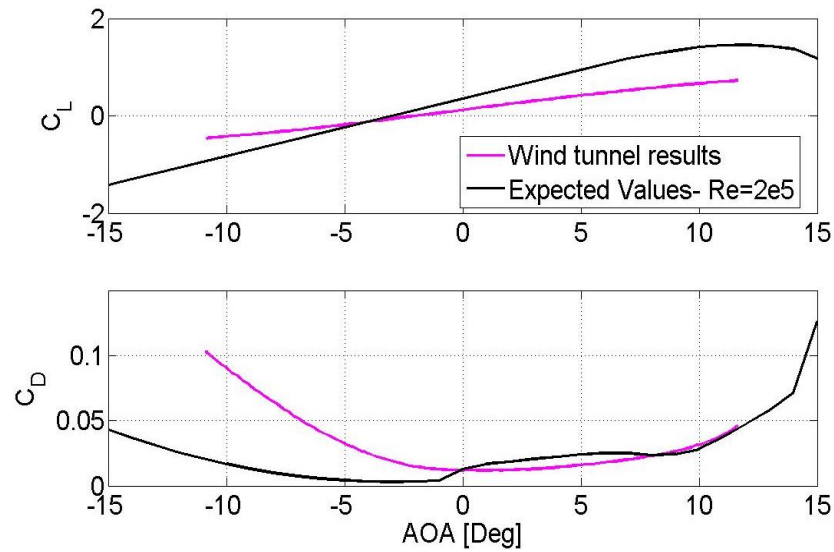
When examining the lift and drag coefficient results at tunnel speed of $45\frac{m}{s}$, there is a good match to the expected values of the airfoil at $Re = 2 \cdot 10^5$.
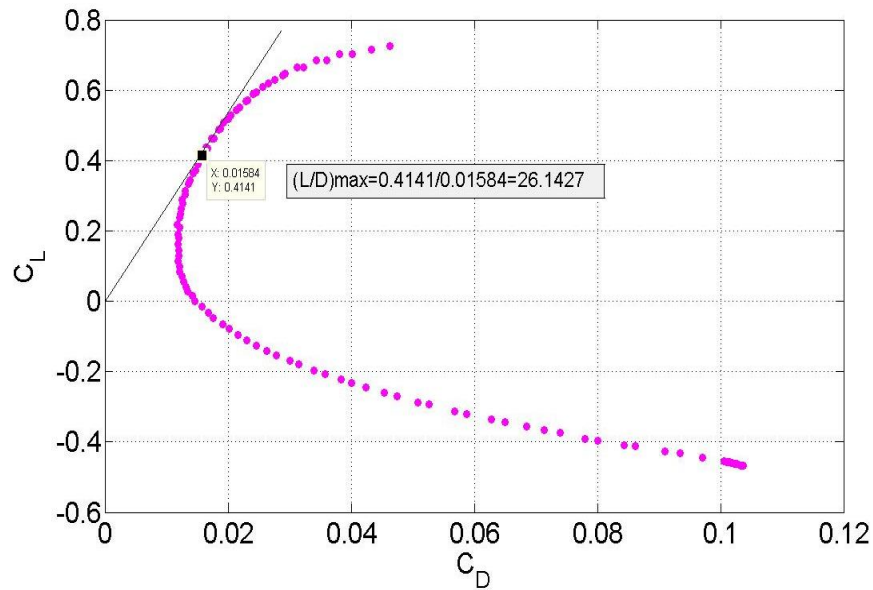
Figure 83

The maximum of the aerodynamic efficiency from the test was 26.14, which was higher than expected.

When comparing the calibration run at $V = 45\frac{m}{s}$ to the expected data, a good match was achieved. The wind tunnel speed was set to $45\frac{m}{s}$ due to the risks to the structure when testing with higher speed. Also, the range of AOA was chosen to be $-10^O < \alpha < 10^O$.

23.2 Splitter ailerons and rudder comparison for yaw

After choosing the speed of the tunnel and the range of AOA, two options for better yaw moment were investigated:

1. Rudders
2. Splitter ailerons

The installation of the control parts is presented in figure 84.

Figure 84

In order to compare the two options, the aerodynamic coefficients were examined (figure 85).
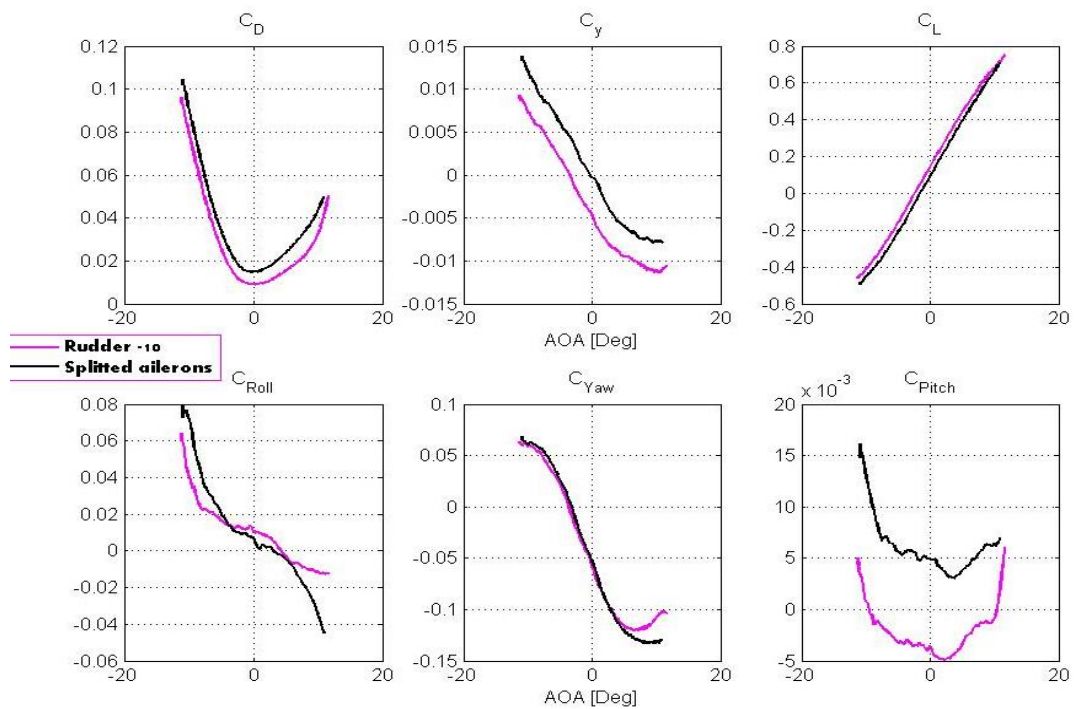
Figure 85

Due to the similar yaw moment coefficient that was achieved using the two options, and the similarity on roll and pitch moments as well, the decision was made using the comparison of the forces coefficients.

When using the rudder for yaw - lower drag, higher lift and lower side force were achieved. The results led to the decision to use rudders for better yaw moment during the actual flight.

23.3 Cavities configurations comparison

Due to the complication of the cavity closing mechanism, the weight of it, and the control problem when designing it, the option of leaving some of the cavities open was investigated.

First, the aerodynamics of the configurations were examined to determine whether the options are possible and then, a performance analysis was carried out to investigate the performance loses.

Five configurations were investigated:

1- All shutters closed
2- Two bottom back shutters open
3- All bottom shutters open
4- Only upper front shutter closed
5- All shutters open

23.3.1 Aerodynamics

The aerodynamic coefficients of the configurations were compared (figure 86).
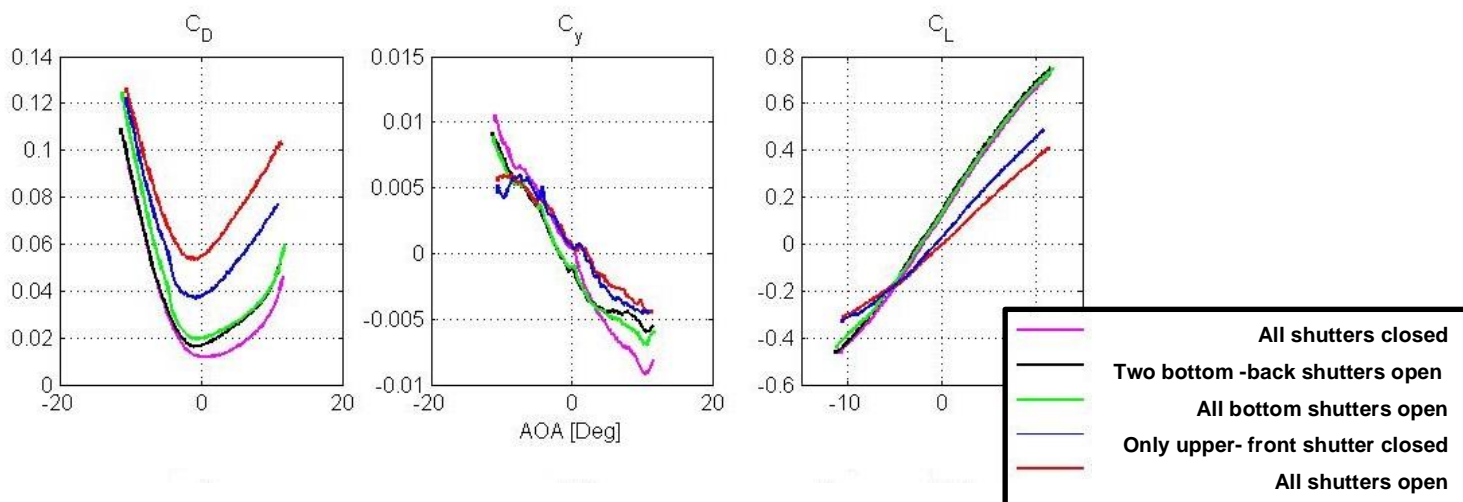
Figure 86

When examining the aerodynamic coefficients differences between the configurations, two main conclusions were achieved from the results:

1- The first three configurations have had similar results.
2- When fewer cavities are closed, the drag increases.

True forces Vs Angle of attack

Legend:
- All shutters closed
- Two bottom -back shutters open
- All bottom shutters open
- Only upper- front shutter closed
- All shutters open
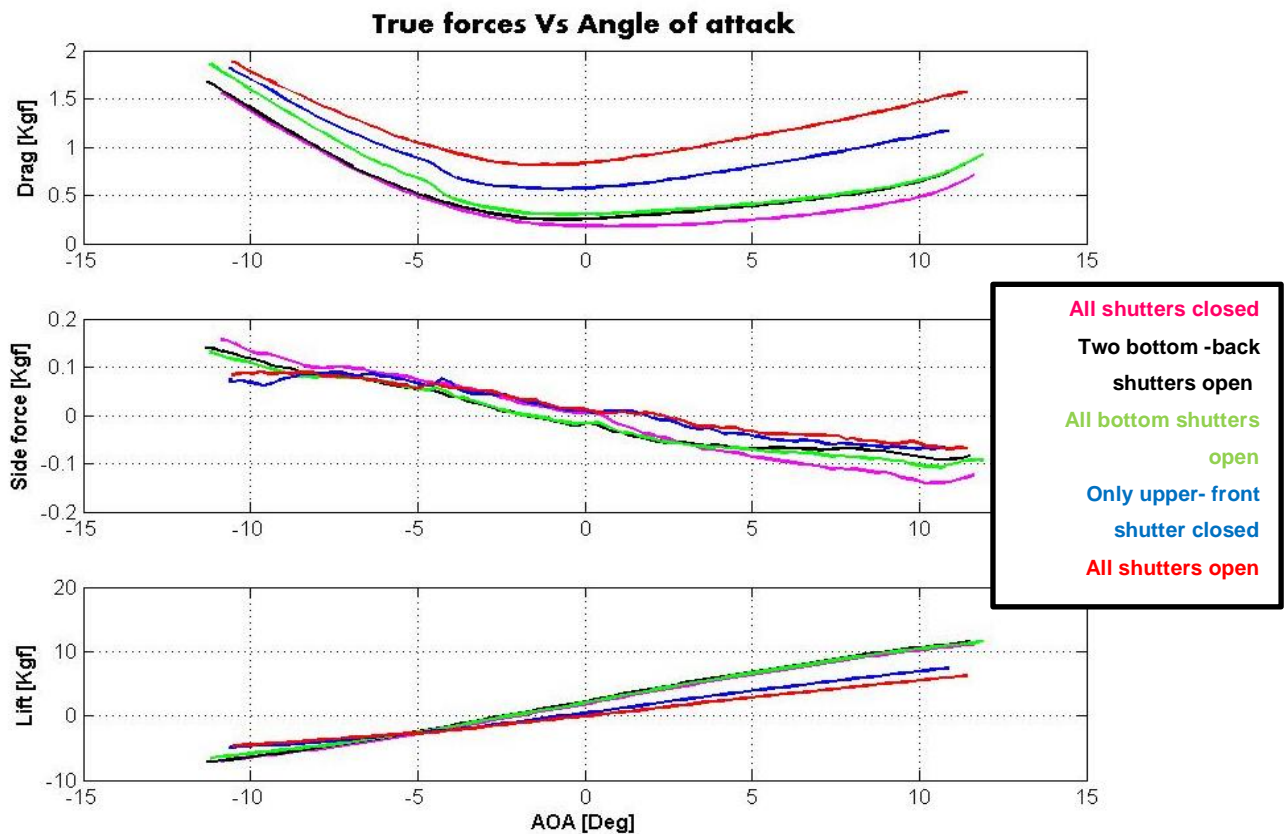
Figure 87

When examining the true forces on the model (figure 86), the results led to rule out the two last options, due to significantly lower lift and higher drag comparing to the first three options.

It was then decided to rule out the 2nd option of two bottom-back shutters opened due to the similarity of it to the option of all bottom shutters opened, and that the purpose was to leave as many cavities opened as possible.

The following comparisons were between two options- the closed configuration and the option of bottom shutters open.

Yaw comparison (figure 87):
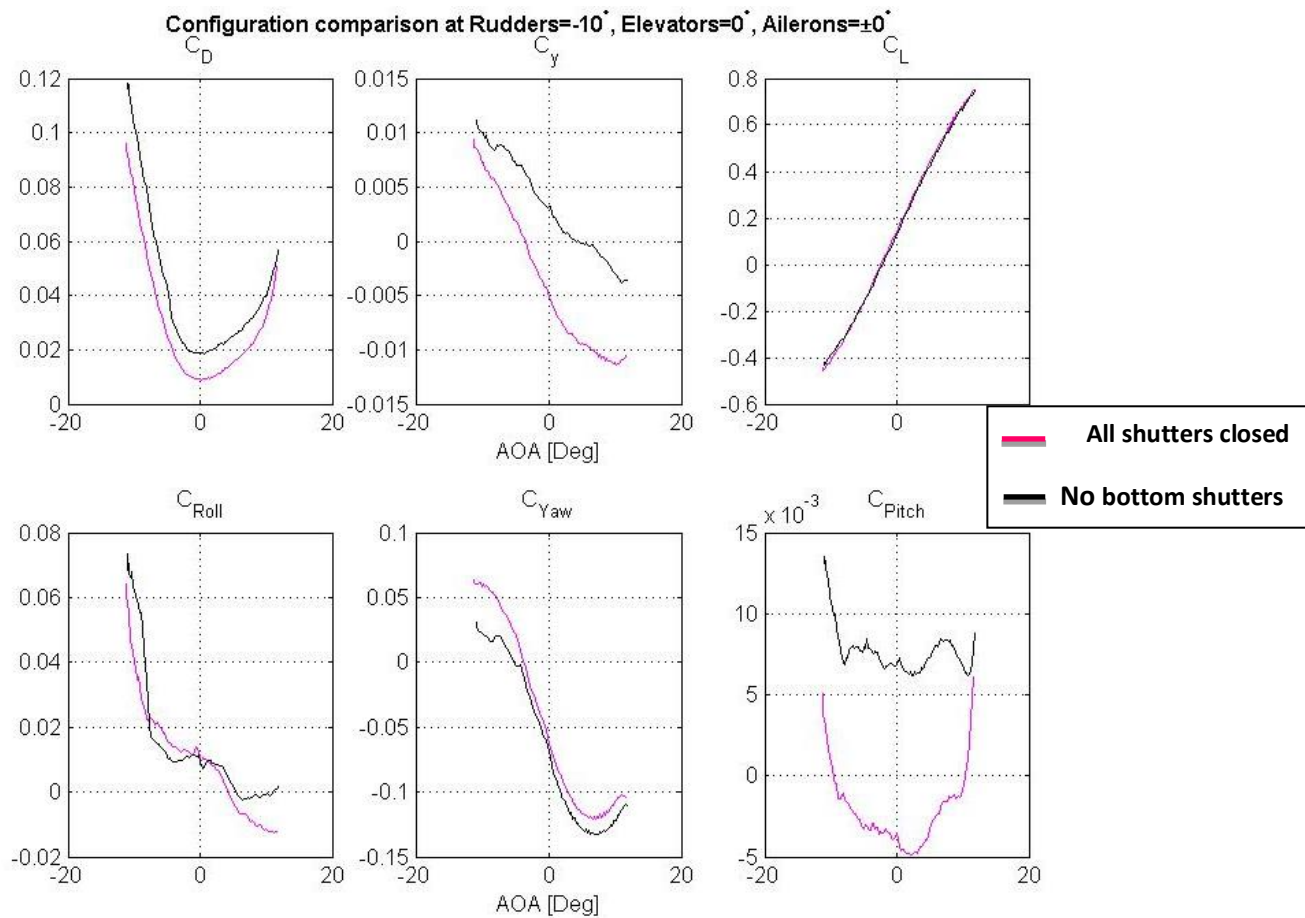
Figure 88

It was noticed that better yaw moment is achieved with closed configuration although the difference was minor. The drag has increased when using the opened bottom covers configuration, as expected. Also, side force has increased significantly. The lift coefficient was very similar, a result that was not expected.

In order to verify the results and rule out any calibration mistake, the experiment was carried out twice. The results repeated themselves.

Pitch (figure 89) and roll (figure 90) comparison:
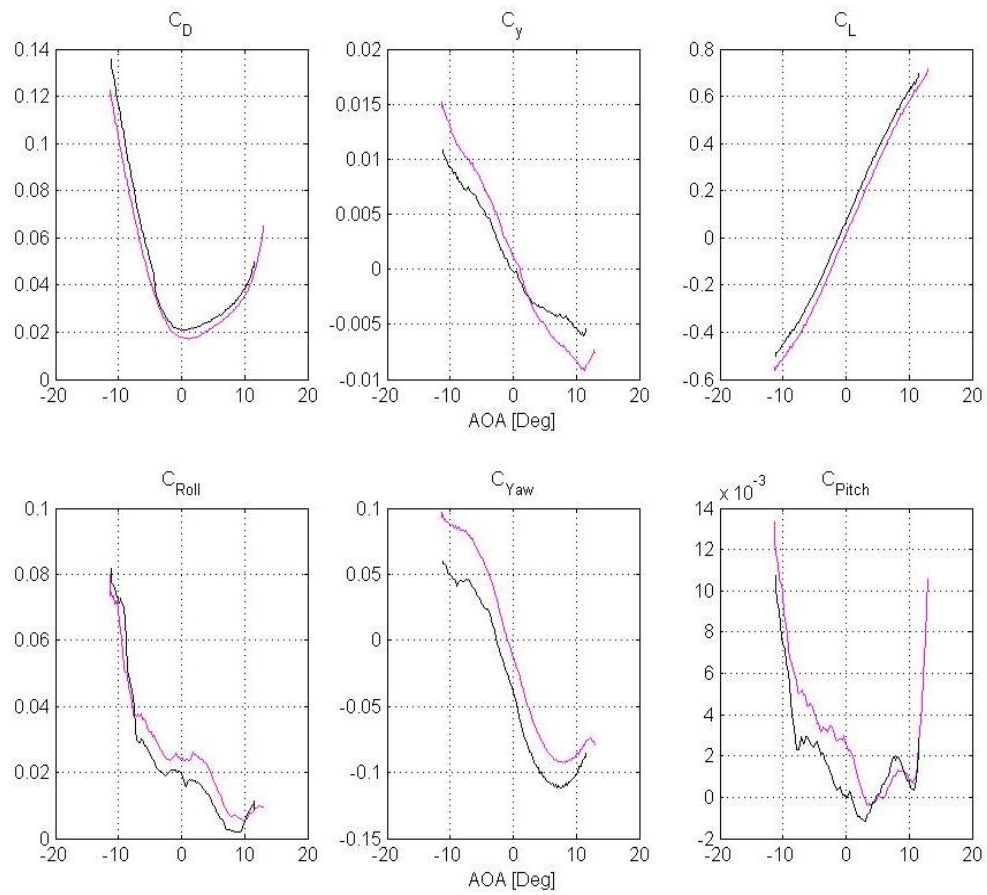
Figure 89
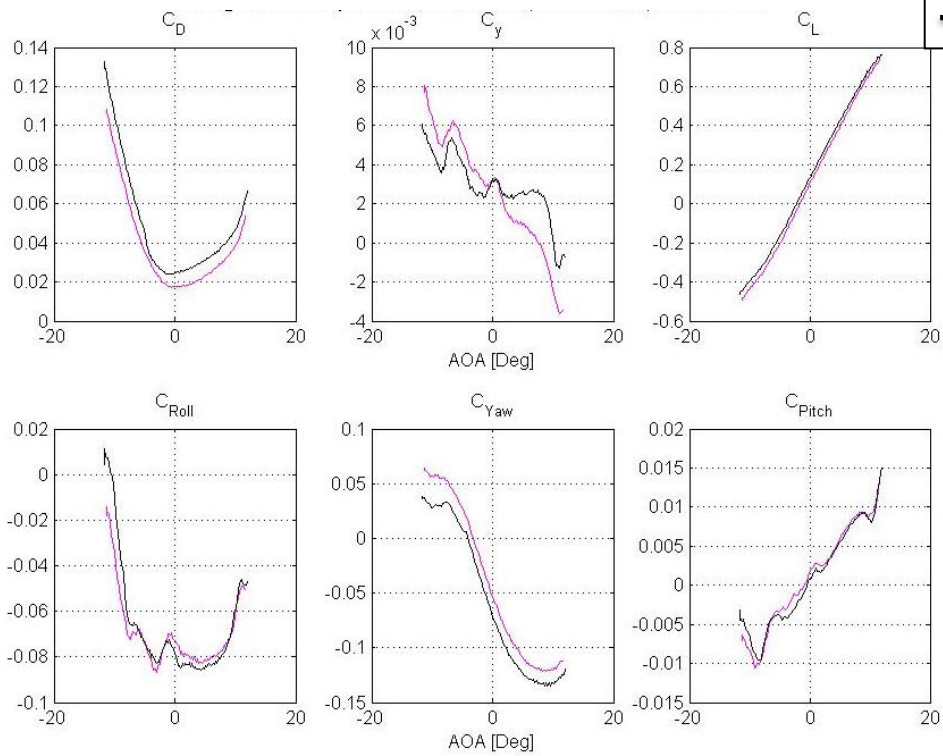
Figure 90

On the pitch and roll experiment, the results were similar. A greater drag was measured on the opened- bottom configuration, a very similar lift and side force were achieved on both configurations.

When examining the moments coefficients- on the pitch comparison- the opened configuration had higher moment values, while on the roll comparison- the results were very similar.

The option of no shutters mechanism on the bottom surface of the UAV was aerodynamically examined for level flight, roll, pitch and yaw maneuvers and was concluded to be reasonably possible.

23.3.2 Performances

After concluding that leaving the bottom of the cavities without any closing mechanism is a reasonable option a performance analysis was carried out to examine the performance loses that this option will lead to. The analysis was also used to determine whether to execute this option.

Stalling speed

		Preliminary analysis results	Experimental Results- All Shutters Closed	Experimental Results- Bottom Shutters Open
Stalling Speed	[Kts]	34.95	27.55	28.02

Table 17

The stalling speed of the UAV (table 17), according to the wind tunnel test, was lower than expected, and was 78% of the expected value. Also, when removing the bottom closing mechanism, the stalling speed was slightly higher (by 1.07%). Overall, the test results were in good match to the theory, and there was no significant change between the configurations.

Aircraft drag at different cruise velocities
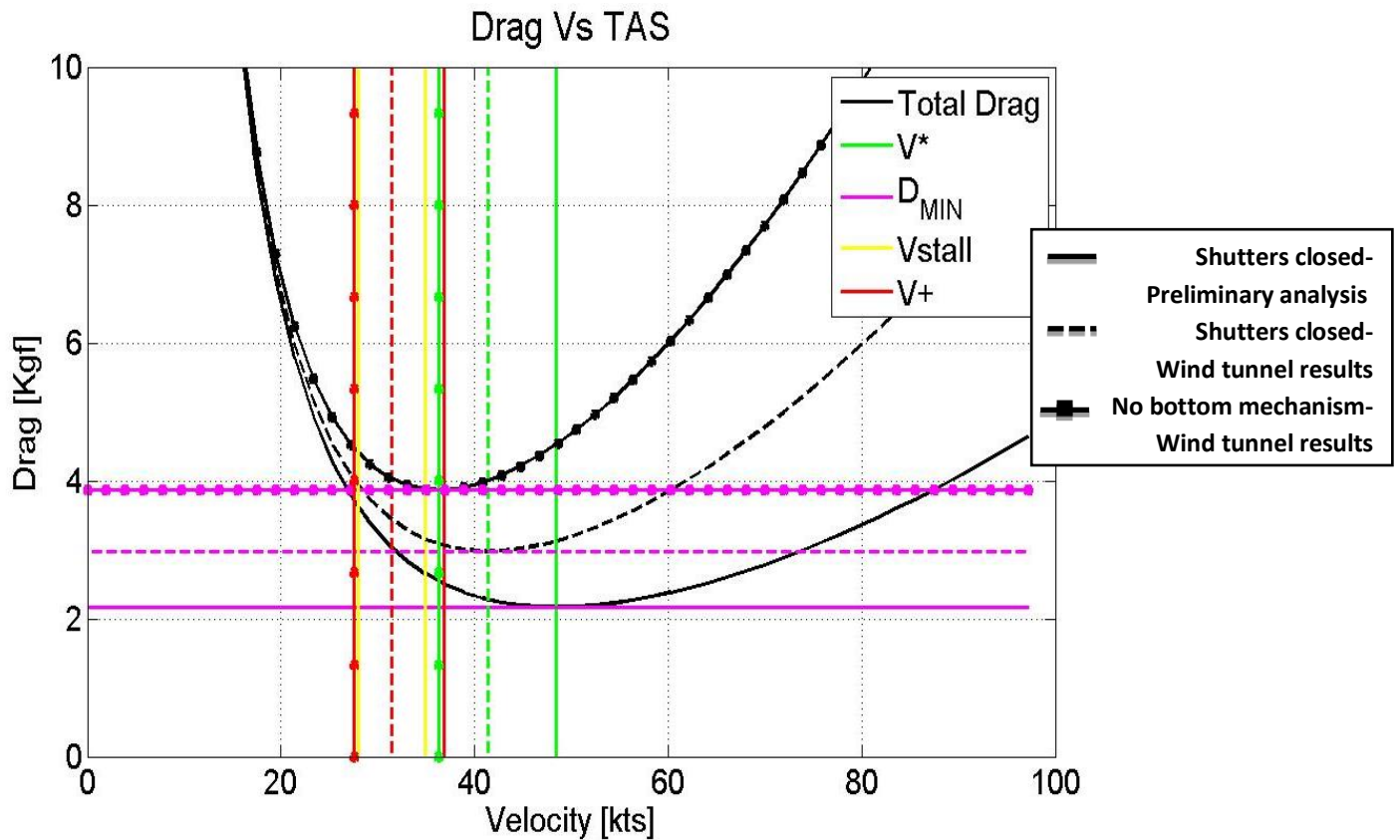
Figure 91

Figure 91 presents the drag on the UAV vs. the flight speed.

The drag on the closed configuration was higher than expected. Also, when removing the bottom closing mechanism the drag rises. Moreover, the velocity of the minimum drag value V^* was lower than expected and decreased when removing the bottom closing mechanism.

Figure 91 showes that the range of velocities in which low drag values are achieved, was smaller with the bottom mechanism removed.

Numerical results (table 18):

		Preliminary analysis results	Experimental Results- All Shutters Closed	Experimental Results- Bottom Shutters Open
Minimum Drag	[Kgf]	2.17	2.97	3.86
At Speed Of	[Kts]	48.46	41.35	36.3

Table 18

Closed configuration drag was 36.8% higher than expected, and at a speed of 41.36 knots, which was 85.3% of the expected value. Overall, when considering the changes that were

75

made to the UAV airfoil due to the wind tunnel limits, there was a good match between the expected values from the theory and the wind tunnel test results.

Required power at different cruise velocities
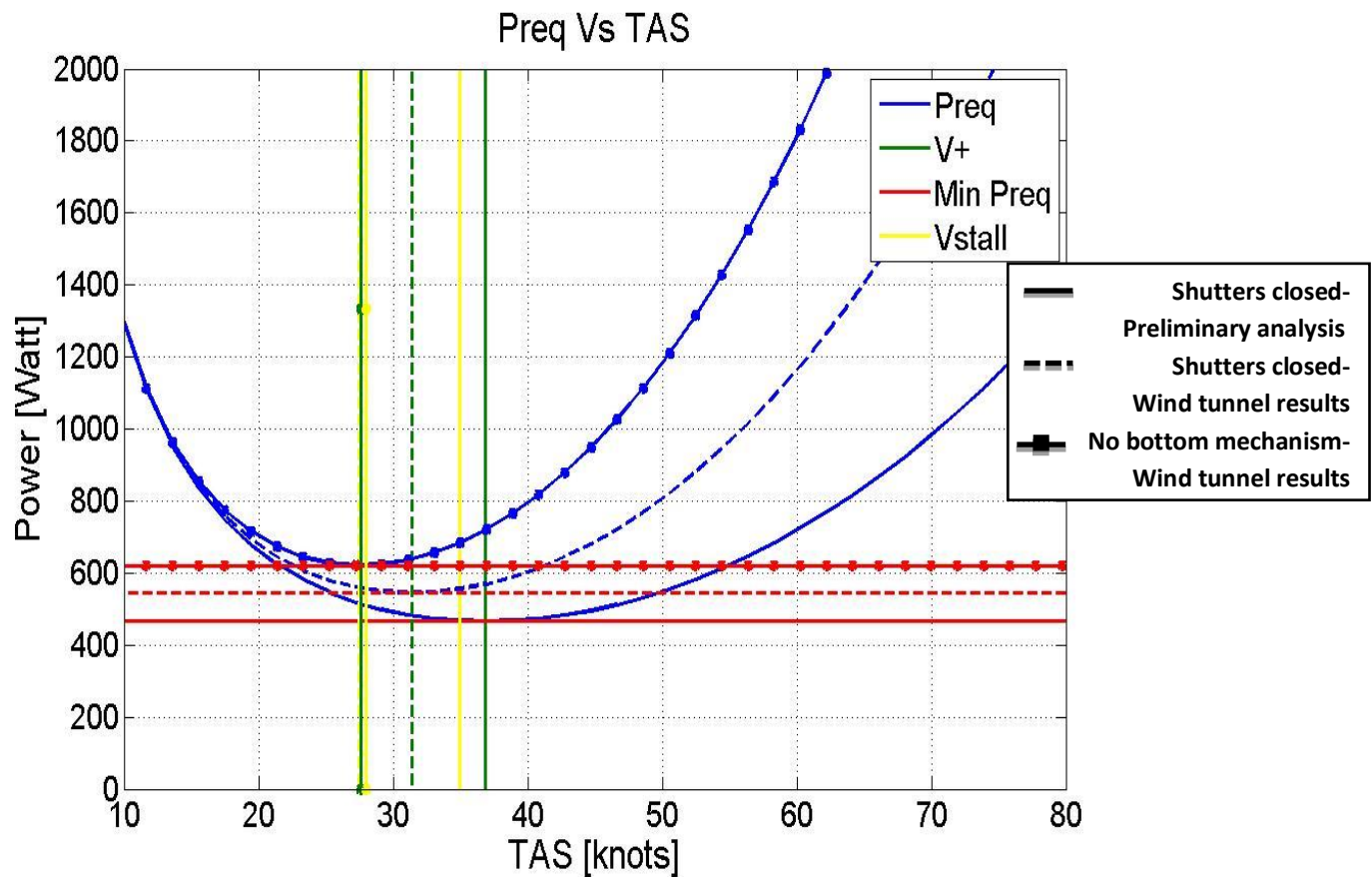
Figure 92

In order to determine whether the horizontal engine will be able to overcome the drag of the UAV, a power comparison was carried out (figure 92). The results showed higher values of required power at lower velocities V^+ for the closed configuration than expected.

Another important result was the fact that the velocity for minimum required power, when investigating the configuration with no bottom closing mechanism, was lower than the stalling velocity. This observation proved the decision to cruise at a higher velocity, which was made in the preliminary performance analysis.

		Preliminary analysis results	Experimental Results- All Shutters Closed	Experimental Results- Bottom Shutters Open	Chosen cruising velocity
Minimum required power	[Watts]	465.2	545.2	621	651.1
At Speed Of	[Kts]	36.8	31.42	27.6	33

Table 19

As seen in table 19, the required power for closed configuration was higher by 17.2% than expected, which was a good match to the expected value. When examining the configuration with no bottom closing mechanism, the minimum required power was 621 watts which was 13.8% higher than the closed configuration.

When choosing the engine for the horizontal flight, it was determined that the engine could supply approximately 700 watts through the entire flight. Choosing a higher cruise velocity of 33 knots led to higher required power value of 651.1 watts, which was lower than the horizontal engine limit. **Overall, it was concluded that the engine will be able to overcome the drag of the UAV with or without the bottom closing mechanism.**

Endurance performance

Due to the fact that the required power has not exceeded the expected power supply of the engine, the endurance has not changed.

When combining the vertical and horizontal flight, the endurance will be approximately 24 minutes.

Range performance

		Preliminary analysis results	Experimental Results- All Shutters Closed	Experimental Results- Bottom Shutters Open
Maximum range	[Km]	30	24.7	20.4
	[Miles]	18.64	15.35	12.7
At Speed Of	[Kts]	48	40	33

Table 20

When investigating the range of the UAV, the results can vary when choosing different cruise velocities. As can be seen in table 20, the closed configuration range was approximately 17% lower than expected.

The range of the UAV was affected by removing the bottom closing mechanism and was approximately 15% lower than the closed configuration, a value of 4Km or 2.5 miles.

23.4 Aerodynamic center

In order to examine the stability of the UAV, the aerodynamic center had to be found.

The aerodynamic center is the location along the chord at which the pitch moment is not affected by the angle of attack. The pitch moment was numerically approximated to a function and derived by the angle of attack.

The result is presented in figure 93.
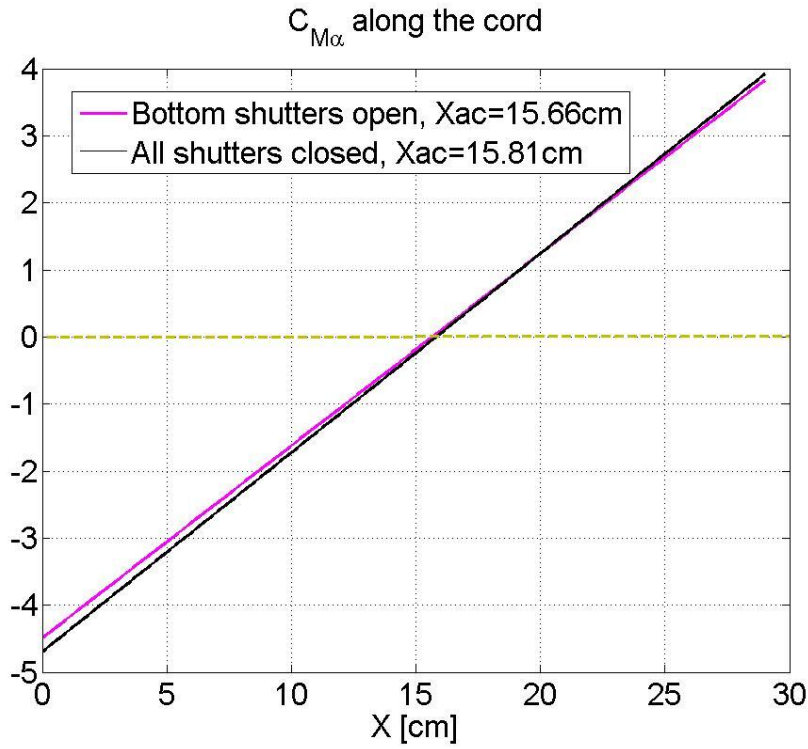
Figure 93

The comparison of the two configuration showed that the difference between the two was less than 0.1% of the chord, which led to the conclusion that removing the bottom closing mechanism of the cavities will not affect the stability of the UAV.

23.5 Control coefficients:

In order to carry out the investigation of the control of the UAV, some coefficients needed to be found.

- $C_{L_\alpha} = 0.0537 \left[1/deg \right]$

- $C_{L_0} = 0.138$

- $C_{D_0} = 0.0197$

- $Y'_\beta = 0.0237 \left[Kgf/deg \right]$

- $L'_\beta = -0.006 \left[Kgf/deg \right]$

- $R'_\beta = 0.7709 \left[\frac{m \cdot Kgf}{deg} \right]$

- $N'_\beta = -0.401 \left[\frac{m \cdot Kgf}{deg} \right]$

24. Summary

The costumer's requirements defined the future product as a small portable UAV, carried and operated by one unskilled person with endurance of 30 and real time video photography capabilities.

Starting with market survey, it was found that a mini-UAV category is suitable for the requirements, including 'toys' that influenced the concept. Due to the survey, it was chosen to combine between a quad-rotor and a flying wing.

This innovatory concept required three vertical motors and one horizontal motor.

As planned, the motors were located inside the wing itself which required a closing mechanism for the cavities of the motors.

After conceptual design was completed, the components and systems were chosen. For propulsion, it was decided to use electric motors which are more quiet and easy to operate. The propellers were chosen to match the motors after considering two and three blades. The choices were verified using theoretical calculation as well as a thrust test. Furthermore, batteries were chosen in order to fit the endurance requirement and weight limitation. The payload was chosen based on the performance and weight.

After all the components and systems were chosen, a calculation of weight and balance was made and the systems were arranged inside the fuselage.

Also, the aerodynamic was analyzed, including airfoil selection, winglets configuration and performance analysis.

The next stage was conceptual and detailed design of the wing structure, choosing materials and creating a 3D model. Moreover, cavity closing system was planned in order to close the cavities of the vertical motors.

The final stage was designing and manufacturing a wind tunnel model and conduction of a wing tunnel test. The test results were analyzed and compered to the performance analysis.

25. Bibliography and literature survey

- John B. Brandt and Michael S. Selig†, **Propeller Performance Data at Low Reynolds Numbers**, University of Illinois, USA, <u>AIAA</u>

- J. Cristofol, Y. Hertienne, M. Lafleur, B. Verguet and S. Vitu, **Tri-rotors UAV Stabilization for Vertical Takeoff and Hovering**, Ecole Centrale d'Electronique, Paris, France

- Dr Stephen D. Prior, Dr Mehmet Karamanoglu, Siddharth Odedra, Mehmet Ali Erbil and Tom Foran, **Development of a Co-Axial Tri-Rotor UAV**, Middlesex University, London, England.

- S.D. Prior, S-T. Shen, M. Karamanoglu, S. Odedra, M. Erbil, C. Barlow and D. Lewis1, **The Future of Battlefield Micro Air Vehicle Systems**, Middlesex University, London, England.

- Jean Koster, Scott Balaban, Andrew Brewer, Chelsea Goodman, Derek Hillery, Cody Humbargar, Mark Johnson, Mikhail Kosyan, Derek Nasso, Julie Price, Eric Serani, Alec Velazco, Tom Wiley, and Richard Zhao, **Hyperion Flying Wing Aircraft Technology**, University of Colorado, USA.

- PRASETYO EDI, NUKMAN YUSOFF and AZNIJAR AHMAD YAZID, **Airfoil Design for Flying Wing UAV (Unmanned Aerial Vehicle)**, University of Malaya, Kuala Lumpur, MALAYSIA.

- Kai Lehmkuehler, KC Wong and Dries Verstraete**, DESIGN AND TEST OF A UAV BLENDED WING BODY CONFIGURATION**, The University of Sydney, Australia.

- Navabalachandran Jayabalan , Low Jun Horng, G. Leng, **Reverse Engineering and Aerodynamic Analysis of a Flying Wing UAV**, National University of Singapore, Singapore.
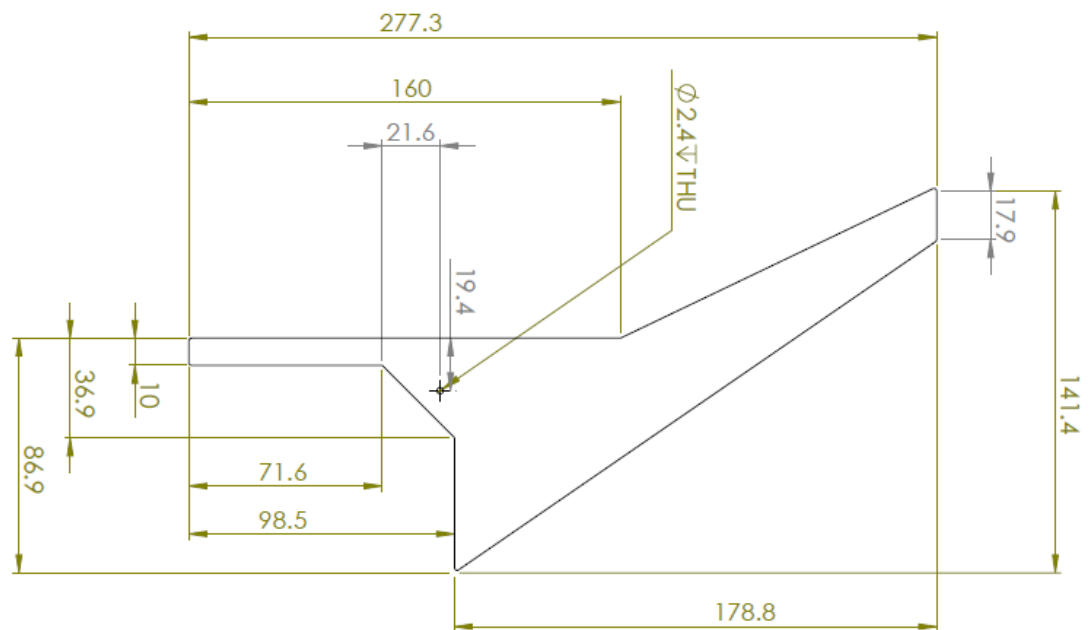
APPENDIX I – Drawings

1. Wind tunnel adapter
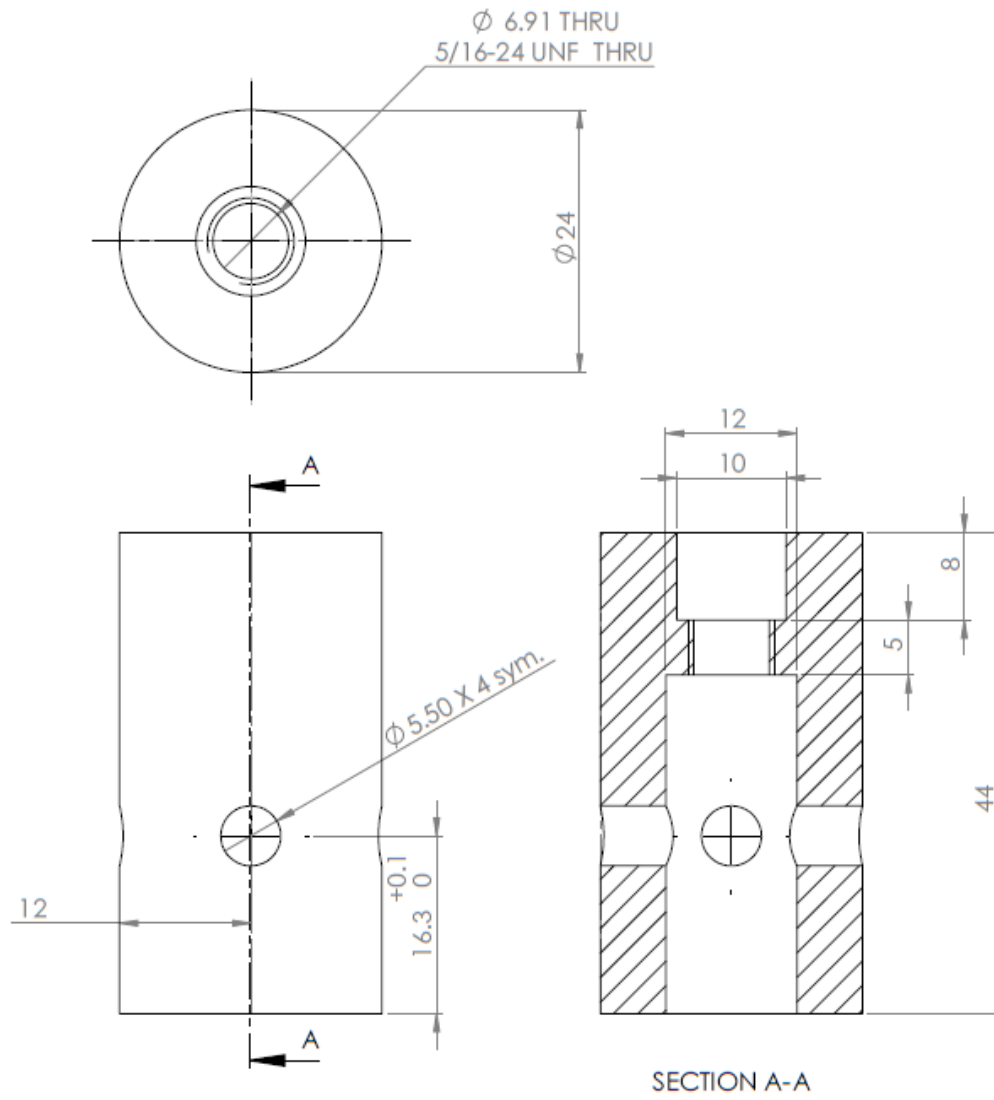
2. Wind tunnel test plan

Priority	Rudders	Elevators	Ailerons	Motor covers	Pitch Plane - α range	Air speed (m/s)	Test No.
1	0	0	0	top+bottom	-20	30	1
1	0	0	0	top+bottom	-20	40	2
1	0	0	0	top+bottom	-20	50	3
1	0	0	-7.5	top+bottom	-20	optimal speed	4
1	0	0	-15	top+bottom	-20		5
1	0	-7.5	0	top+bottom	-20		6
1	0	-15	0	top+bottom	-20		7
1	0	7.5	0	top+bottom	-20		8
1	0	15	0	top+bottom	-20		9
1	-5	0	0	top+bottom	-20		10
1	-10	0	0	top+bottom	-20		11
1	5	0	0	top+bottom	-20		12
1	10	0	0	top+bottom	-20		13
1	0	0	split aileron	top+bottom	-20		14
1	0	0	-7.5	top only	-20	optimal speed	15
1	0	0	-15	top only	-20		16
0	0	-7.5	0	top only	-20		17
0	0	-15	0	top only	-20		18
1	0	7.5	0	top only	-20		19
1	0	15	0	top only	-20		20
0	-5	0	0	top only	-20		21
0	-10	0	0	top only	-20		22
1	5	0	0	top only	-20		23
1	10	0	0	top only	-20		24
1	0	0	split aileron	top only	-20		25
1	0	0	-7.5	none	-20	optimal speed	26
1	0	0	-15	none	-20		27
0	0	-7.5	0	none	-20		28
0	0	-15	0	none	-20		29
1	0	7.5	0	none	-20		30
1	0	15	0	none	-20		31
0	-5	0	0	none	-20		32
0	-10	0	0	none	-20		33
1	5	0	0	none	-20		34
1	10	0	0	none	-20		35
1	0	0	split aileron	none	-20		36
Preference	Rudders	Elevators	Ailerons	Motor covers	Yaw Plane - β range	Air speed (m/s)	Test No.
1	0	0	0	top+bottom	-20	optimal speed	37
1	0	0	split aileron	top+bottom	-20		38
1	-5	0	0	top+bottom	-20	optimal speed	39
1	-10	0	0	top+bottom	-20		40
1	5	0	0	top+bottom	-20		41
1	10	0	0	top+bottom	-20		42
0	-5	0	0	top only	-20	optimal speed	43
0	-10	0	0	top only	-20		44
1	5	0	0	top only	-20		45
1	10	0	0	top only	-20		46
0	-5	0	0	none	-20	optimal speed	47
0	-10	0	0	none	-20		48
1	5	0	0	none	-20		49
1	10	0	0	none	-21		50

3. Wind tunnel model wing plate

4. Wind tunnel model – Assembly